Efficient option pricing for Rough Bergomi model

1 The goal and outline of the project

The main goal of the project is to design a fast option pricer, based on multi-index stochastic collocation (MISC), for options whose dynamics follow rBergomi model. We may later investigate QMC.

2 Review of literature

Rough stochastic volatility models in which the trajectories of volatility are less regular than those of the standard Brownian motion, have gained popularity among academics and practitioners. As shown in [15, 2], replacing standard Brownian motion by its (rough) fractional, counterpart in volatility models allows to capture and explain crucial phenomena observed both in volatility time-series and in the implied volatility of option prices. Since then, rough volatility models have become the go-to models capable of reproducing stylised facts of financial markets and of providing a unifying theory with implications branching across financial disciplines.

From a practical perspective the natural question arises: What does the mantra of rough volatility mean for a trader with a view to hedging his positions? Due to the non-Markovian nature of the fractional driver, hedging under rough volatility poses a delicate challenge making even the very definition of hedging strategies difficult. In particular, partial differential equations can no longer be used, and simulation is the only available route. Despite the availability of efficient Monte Carlo schemes [6, 16, 21] , pricing and model calibration in rough volatility models remain time consuming.

We focus here on the option pricing problem in rough volatility models.

The extension of the Black-Scholes model, in which volatility is assumed to be constant, to the case where the volatility is stochastic has proved to be successful in explaining certain phenomena observed in option price data, in particular the implied volatility smile. The main shortcoming of such stochastic volatility models, however, is that they are unable to capture the true steepness of the implied volatility smile close to maturity. While choosing to add jumps to stock price models, for example modelling the stock price process as an exponential Lévy process, does indeed produce steeper implied volatility smiles, the question of the presence of jumps in stock price processes remains controversial [1, 9].

As an alternative to exponential Lévy and classical stochastic volatility models, one may choose a fractional Brownian motion, or a process with similar fine properties, to drive the volatility process, rather than a standard Brownian motion. Since volatility is neither directly observable nor tradable, the issue of arbitrage that is sometimes associated to fractional Brownian motion does not arise in this case. A fractional Brownian motion is a centred Gaussian process, whose covariance

structure depends on the Hurst parameter $H \in (0,1)$. If $H \in (0,1/2)$, then the fractional Brownian motion has negatively correlated increments and "rough" sample paths, and if $H \in (1/2,1)$ then it has positively correlated increments and "smooth" sample paths, when compared with a standard Brownian motion, which is recovered by taking $H = 1/2$. There has been a resurgent interest in fractional Brownian motion and related processes within the mathematical finance community in recent years. In particular, Gatheral, Jaisson and Rosenbaum [15] carry out an empirical study that suggests that the log volatility behaves at short time scales in a manner similar to a fractional Brownian motion, in terms of its covariance structure, with Hurst parameter $H \approx 0.1$. This finding is corroborated by Bennedsen, Lunde and Pakkanen [5], who study over a thousand individual US equities and find that the Hurst parameter H lies in $(0,1/2)$ for each equity. In addition, such so-called "rough" volatility models are able to capture the observed steepness of small-time implied volatility smiles and the term structure of at-the-money skew much better than classical stochastic volatility models.

Following [15], Bayer, Friz and Gatheral [2] propose the so-called rough Bergomi model, which they then use to price options on integrated volatility and on the underlying itself. The advantage of their model is that it captures the "rough" behaviour of log volatility, in accordance with [5, 15], as well as fits observed implied volatility smiles better than traditional Markovian stochastic volatility models, most notably in the close-to-maturity case. At the moment, the only known method for pricing mere vanilla options, and computing the corresponding implied volatility smiles, in this setting is Monte Carlo simulation. Recent advances in simulation methods for the rough Bergomi model have been acheived in [6, 17], and also more analytical results of option pricing and implied volatility under this model has been done in [18, 4, 12]. For isntance, in [18] they characterise the small-time behaviour of implied volatility using large deviations theory and related results, concerning the small-time near-the-money skew, have been obtained by Bayer, Friz, Gulisashvili, Horvath and Stemper [4].

The work of Gatheral, Jaisson and Rosenbaum [15] has brought a gradual shift in volatility modeling, leading away from classical diffusive stochastic volatility models towards so-called rough volatility models [15, 2]. It essentially describes a family of (continuous-path) stochastic volatility models where the driving noise of the volatility process has H older regularity lower than Brownian motion, typically achieved by modeling the fundamental noise innovations of the volatility process as a fractional Brownian motion with Hurst exponent (and hence H older regularity)$H < 1/2$. A major advantage of such rough volatility models is the fact that they effectively capture several stylized facts of financial markets both from a statistical [15, 5] and an option-pricing point of view [2]. In particular, with regards to the latter point of view, a widely observed empirical phenomenon in equity markets is the steepness of the smile on the short end" describing the fact that as time to maturity becomes small the empirical implied volatility skew follows a power law with negative exponent, and thus becomes arbitrarily large near zero. While standard stochastic volatility models with continuous paths struggle to capture this phenomenon, predicting instead a constant at-the-money implied volatility behaviour on he short end [13], models in the fractional stochastic volatility family (and more specifically so-called rough volatility models) constitute a class, well-tailored to fit empirical implied volatilities for short dated options.

Typically, the popularity of asset pricing models hinges on the availability of efficient numerical pricing methods. In the case of diffusions, these include Monte Carlo estimators, PDE discretization schemes, asymptotic expansions and transform methods. With fractional Brownian motion being the prime example of a process beyond the semimartingale framework, most currently prevalent

option pricing methods -particularly the ones assuming semimartingality or Markovianity - may not easily carry over to the rough setting. In fact, the memory property (aka non-Markovianity) of fractional Brownian motion rules out PDE methods, heat kernel methods and all related methods involving a Feynman-Kac-type Ansatz. Previous work has thus focused on finding efficient Monte Carlo simulation schemes [2, 6, 3] or - in the special case of the Rough Heston model - on an explicit formula for the characteristic function of the log-price (see [11]), thus in this particular model making pricing amenable to Fourier based methods.

It is a well-documented fact on Equity markets (see for instance Chapter 5 of [13]) that standard (Itô) stochastic models with continuous paths are not able to capture the observed steepness of the left wing of the smile when the maturity becomes small. To remedy this, several authors have suggested the addition of jumps, either in the form of an independent Lévy process or within the more general framework of affine diffusions. Jumps (in the stock price dynamics) imply an explosive behaviour for the small maturity smile and are better able to capture the observed steepness of the small-maturity implied volatility smile. In particular, Tankov [24] showed that, for exponential Lévy models with Levy measure supported on the whole real line, the squared implied volatility smile explodes as $\sigma_\tau^2(k) \sim k^2/(2\tau \log \tau)$, as the maturity tends to zero, where k represents the log-moneyness. Such a small-maturity behaviour of the smile is not only captured by jump-based models, but rough volatility (non-Markovian) models, where the stochastic volatility component is driven by a fractional Brownian motion, are in fact also able to reflect this property of the data. In a series of papers several authors [4, 12, 18] have indeed proved that, when the Hurst index of the fractional Brownian motion lies within $(0, 1/2)$, then the implied volatility explodes at a rate of $\tau^{H-1/2}$ as the maturity tends to zero.

The last few years have seen renewed interest in stochastic volatility models driven by fractional Brownian motion (fBM) or other self-similar Gaussian processes (see [2, 15]). Recall that fractional Brownian motion B^H is a centered self-similar Gaussian process with stationary increments, which depends on a parameter $H \in (0, 1)$ called the Hurst index, and B^H is persistent (i.e., more likely to keep a trend than to break it) when $H > 1/2$ and antipersistent when $H < 1/2$ (i.e., if B^H was increasing in the past, B^H is more likely to decrease in the future, and vice versa).

Gatheral, Jaisson, and Rosenbaum [15] provide strong empirical justification for such models; in particular, they argue that log-volatility in practice behaves essentially as fBM with the Hurst exponent $H \approx 0.1$ at any reasonable time scale (see also [14]). In particular, Gatheral, Jaisson, and Rosenbaum [15] advocate a model in which the volatility is the exponential of a fractional OU process with small mean-reversion parameter.

Recently, Bayer, Friz, and Gatheral [2] analyze the rough Bergomi variance curve model, which is shown to fit SPX option prices significantly better than conventional Markovian stochastic volatility models, and with fewer parameters.

A number of empirical studies suggest that the volatility process possesses long- and short-range dependence, that is, the correlation function of the volatility process has decay that is a fractional power of the time offset.

The concept of Rough Fractional Stochastic Volatility (RFSV) is put forward in [2, 15]. Here a model with log-volatility modeled by an fBm is motivated by analysis of market data, which they state provide strong support for a value for the Hurst exponent H around 0.1. As explained above, small values for H correspond to very rough processes. The authors discuss issues related to changing from physical to pricing measure and using simulated prices to

t well the implied volatility surface in the case of the S&P 500 index with few parameters. They

argue that the fractional model generates strong skews or "smiles" in the implied volatility even for very short time to maturity so that this modeling provides an alternative to using jumps to model such an effect.

3 Background on Gaussian and fBM processes

A zero-mean real-valued Gaussian process $(Z_t)_{t\geq 0}$ is a stochastic process such that on any finite subset $\{t_1, \dots t_n\} \subset \mathbb{R}, (Z_{t_1}, \dots, Z_{t_n})$ has a multivariate normal distribution with mean zero. The law of a Gaussian process is entirely determined by the covariance function $K(s,t) = \mathrm{E}\left[Z_t Z_s\right]$ and Z induces a Gaussian probability measure on $(E, \mathcal{B}(E))$, where E denotes the Banach space $C_0[0,1]$ with the usual sup norm topology (see, e.g., section 3.1.1 of [8] for details).

Fractional Brownian motion (fBM) is a natural generalization of standard Brownian motion which preserves the properties of stationary increments, self-similarity, and Gaussian finite-dimensional distributions, but it has a more complex dependence structure which exhibits long-range dependence when $H > 1/2$. In this section, we recall the definition and summarize the basic properties of fBM.

A zero-mean Gaussian process B_t^H is called standard fractional Brownian motion (fBM) with Hurst parameter $H \in (0,1)$ if it has covariance function

$$R_H = \mathrm{E}\left[B_t^H B_s^H\right] - \mathrm{E}\left[B_t^H\right]\mathrm{E}\left[B_s^H\right] = \frac{1}{2}\left(|t|^{2H} + |s|^{2H} - |t-s|^{2H}\right). \tag{1}$$

In order to specify the distribution of a Gaussian process, it is enough to specify its mean and its covariance function; therefore, for each H, the law of B^H is uniquely determined by $R^H(s,t)$. However, this definition by itself does not guarantee the existence of fBM; to show that fBM exists, one needs to verify that the covariance function is nonnegative definite.

We now recall some fundamental properties of fBM (see also Figure 1):

- fBM is continuous a.s. and H-self-similar (H-ss), i.e., for $a > 0, (B_{at})_{t\geq 0} \stackrel{(d)}{=} a^H (B_t)_{t\geq 0}$ where $\stackrel{(d)}{=}$ means both processes have the same finite-dimensional distributions. For $H \neq 1/2$, B^H does not have independent increments; for $H = 1/2, B_t^H$ is the standard Brownian motion.
- From (1), we see that
$$\mathrm{E}\left[B_t^H - B_s^H)^2\right] = |t-s|^{2H},$$
so $B_t^H - B_s^H \sim \mathcal{N}(0, |t-s|^{2H})$; thus B^H has stationary increments.
- If we set $X_n = B_n^H - B_{n-1}^H$, then X_n is a discrete-time Gaussian process with covariance function
$$\begin{aligned}\rho_n &= \mathrm{E}\left[X_{k+n X_n}\right] = \mathrm{E}\left[\left(B_{k+n}^H - B_{k+n-1}^H\right)\left(B_k^H - B_{k-1}^H\right)\right] \\ &\sim H(2H-1)n^{2H-2} \quad (n \to \infty),\end{aligned}$$
and thus (by convexity of the function $g(n) = n^{2H}$), we see that two increments the form $B_k - B_{k-1}$ and $B_{k+n} - B_{k+n-1}$ are positively correlated if $H \in (1/2, 1)$ and negatively

correlated if $H \in (0, 1/2)$. Thus B^H is persistent (i.e., it is more likely to keep a trend than to break it) when $H > 1/2$, the relatively stronger positive correlation for the consecutive increments of the associated fBm process with increasing H values gives a relatively smoother process whose correlations decay relatively slowly.And antipersistent when $H < 1/2$ (i.e., if B^H was increasing in the past, it is more likely to decrease in the future, and vice versa). The enhanced negative correlation with smaller Hurst exponent gives a relatively rougher process.

- If $H \in (1/2, 1)$, we can show that $\sum_{n=1}^{\infty} \rho_n = \infty$, which means that the process exhibits long-range dependence, but if $H \in (0, 1/2)$, then $\sum_{n=1}^{\infty} \rho_n < \infty$.
- Using that $\mathrm{E}\left[(B_t^H - B_s^H)^2\right] = (t-s)^{2H}$, we can show that sample paths of B^H are α-H older continuous for all $\alpha \in (0, H)$.
- fBM is the only self-similar Gaussian process with stationary increments (see, e.g., [20]), and for $H \neq 1/2$, B_t^H is neither a Markov process nor a semimartingale (see, e.g., [22]).

More details regarding the fBm processes we refer, respectively, to [7, 10, 19].

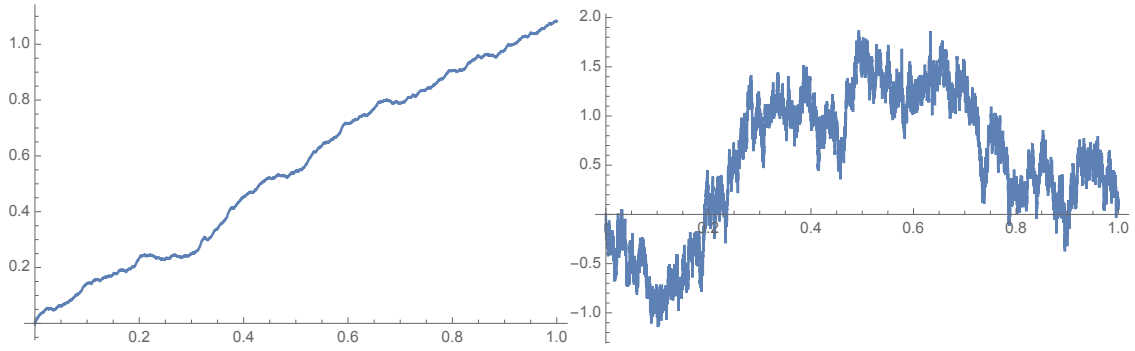

(a) (b)

Figure 1: Monte Carlo simulation of fBM for $H = 0.9$ (left) and $H = 0.3$ (right).

4 The rBergomi model

We use the rBergomi model(rough stochastic volatility model) for the price process S_t as defined in [2], normalized to $r = 0$ and, which is defined by

$$dS_t = \sqrt{v_t(\tilde{W}^H)} S_t dZ_t, \tag{2}$$

$$v_t = \xi_0(t) \exp\left(\eta \tilde{W}_t^H - \frac{1}{2}\eta^2 t^{2H}\right), \tag{3}$$

where for $0 < H < 1$, we have $\tilde{W}^H$ is a certain Volterra process, defined by

$$\tilde{W}_t^H = \int_0^t K^H(t, s) dW_s^1, \quad t \geq 0 \tag{4}$$

where the kernel $K^H : \mathbb{R}_+ \times \mathbb{R}_+ \to \mathbb{R}_+$ reads

$$K^H(t,s) = \sqrt{2H}\,|t-s|^{H-1/2}, \quad \forall\, 0 \le s \le t. \tag{5}$$

We note that the map $s \to K^H(s,t)$ belongs to L^2, so that the stochastic integral (4) is well defined.

W^1, Z denote two *correlated* standard Brownian motions with correlation $\rho \in [-1,1]$, so that

$$Z := \rho W^1 + \overline{\rho} W^2 \equiv \rho W^1 + \sqrt{1-\rho^2} W^2, \tag{6}$$

where (W^1, W^2) are two independent standard Brownian motions, Therefore, Eq 2 can be written as

$$\begin{aligned} S_t &= S_0 \exp\left(\int_0^t \sqrt{v(s)} dZ(s) - \frac{1}{2}\int_0^t v(s) ds\right), \quad S_0 > 0 \\ v(u) &= \xi_0 \exp\left(\eta \tilde{W}_u^H - \frac{\eta^2}{2} u^H\right), \quad \xi_0 > 0 \end{aligned} \tag{7}$$

The filtration $(\mathcal{F}_t)_{t\ge 0}$ can here be taken as the one generated by the two-dimensional Brownian motion (W^1, W^2). The stock price process S is clearly then a local $(\mathcal{F}_t)_{t\ge 0}$-martingale and a supermartingale, therefore integrable.

We refer to v_u as the variance process, where $\xi_0(u) = \mathrm{E}[v_u] \in \mathcal{F}_0$ a.s. the forward variance curve. $\tilde{W}^H$ is a centered, locally $(H-\epsilon)$- Hölder continuous, Gaussian process with $\mathrm{var}[\tilde{W}_t^H] = t^{2H}$.

In [2], the approach consists in sampling the Gaussian process Z and $\tilde{W}^H$ on a discrete time grid using exact simulation and then approximating S and v using Euler discretization.

Assuming $S_0 = 1$, and using the conditioning argument on the σ-algebra generated by W^1 (argument first used by [23] in the context of Markovian SV models), we can show that the call price is given by

$$\begin{aligned} C_{RB}(T,K) &= E\left[(S_T - K)^+\right] \\ &= \mathrm{E}\left[\mathrm{E}\left[(S_T-K)^+ \mid \sigma(W^1(t), t \le T)\right]\right] \\ &= E\left[C_{BS}\left(S_0 = \exp\left(\rho\int_0^T \sqrt{v_t} dW_t^1 - \frac{1}{2}\rho^2\int_0^T v_t dt\right),\ K = K,\ T = 1,\ \sigma^2 = (1-\rho^2)\int_0^T v_t dt\right)\right], \end{aligned} \tag{8}$$

where C_{BS} denotes the Black-Scholes price.

In fact, if we use the orthogonal decomposition of S_t into S_t^1 and S_t^2, where

$$S_t^1 := \mathcal{E}\{\rho\int_0^t \sqrt{v_s} dW_s^1\},\ S_t^2 := \mathcal{E}\{\sqrt{1-\rho^2}\int_0^t \sqrt{v_s} dW_s^2\}, \tag{9}$$

where $\mathcal{E}()$ denotes the stochastic exponential, then, we obtain

$$\log S_t \mid \mathcal{F}_t^1 \sim \mathcal{N}\left(\log S_t^1 - \frac{1}{2}(1-\rho^2)\int_0^t v_s ds, (1-\rho^2)\int_0^t v_s ds\right), \tag{10}$$

where $\mathcal{F}_t^1 = \sigma\{W_s^1 : s \le t\}$. Therefore, we obtain (8).

5 Simulation of the rBergomi model

The main challenge is the computation of $S = \int_0^T \sqrt{v_t} dW_t^1$ and $V = \int_0^T v_t dt$. As was mentioned in [3], we may try to avoid any sampling related to W^2 by a brute-force approach that consists in simulating a scalar Brownian motion W^1, followed by computing $\tilde{W}^H = \int K dW^1$ by Itô/Riemann Stieltjes approximations of (S, V). However, this is not advisable given the singularity of the Volterra kernel $K(s,t)$ at the diagonal $s = t$. Therefore, one needs to jointly simulate the two-dimensional Gaussian process $(W_t^1, \tilde{W}_t^H : 0 \leq t \leq T)$, resulting in $W_{t_1}^1, \ldots, W_{t_N}$ and $\tilde{W}_{t_1}^H, \ldots, \tilde{W}_{t_N}^H$ along a given grid $t_1 < \cdots < t_N$. There are essentially three possible ways to achieve this:

1. Euler discretization of the integral defining $\tilde{W}^H$ together with classical simulation of increments of W^1. This is horribly inefficient because the integral is singular and adaptivity probably does not help, as the singularity moves with time. For this method, we need an N-dimensional random Gaussian input vector to produce one (approximate, inaccurate) sample of $W_{t_1}^1, \ldots, W_{t_N}^1, \tilde{W}_{t_1}^H, \ldots, \tilde{W}_{t_N}$.

2. Given that $W_{t_1}^1, \ldots, W_{t_N}^1, \tilde{W}_{t_1}^H, \ldots, \tilde{W}_{t_N}$ together forms a $(2N)$-dimensional Gaussian random vector with computable covariance matrix. We can use Cholesky decomposition of the covariance matrix to produce exact samples of $W_{t_1}^1, \ldots, W_{t_N}^1, \tilde{W}_{t_1}^H, \ldots, \tilde{W}_{t_N}$, but unlike the first way, we need $2N$-dimensional Gaussian random vectors as input. This method is exact but slow (See Section 4 in [4]).

3. The hybrid scheme of [6] uses a different approach, which is essentially based on Euler discretization as the first way but crucially improved by moment matching for the singular term in the left point rule. It is also inexact in the sense that samples produced here do not exactly have the distribution of $W_{t_1}^1, \ldots, W_{t_N}^1, \tilde{W}_{t_1}^H, \ldots, \tilde{W}_{t_N}$,however they are much more accurate then samples produced from method 1), but much faster than method 2). As in method 2), in this case we need a $2N$-dimensional Gaussian random input vector to produce one sample of $W_{t_1}^1, \ldots, W_{t_N}^1, \tilde{W}_{t_1}^H, \ldots, \tilde{W}_{t_N}$.

In this project, we adopt the last approach for the simulation of the rBergomi model.

6 Numerical tests

6.1 Integrand plotting wrt different random inputs

In this section, we plot the integrand, given by the term inside the expectation in (8)(including the Gaussian density), wrt different random inputs (W_1, W_2) (W_2 stands for W^{perp} in the code). This is important to check if we need a measure change and if needed for which variables. We show the results for $H = 0.43$ and $H = 0.07$ and for two scenarios of number of time steps $N \in \{2, 4\}$. We also show the two dimensional plots (See figures (24,4,7,9,8). As it seems from the plots, we may just need change of measure wrt to W_1 coordinates and we do not need a measure chnage for W_2 coordinates.

6.1.1 N=2, H=0.07

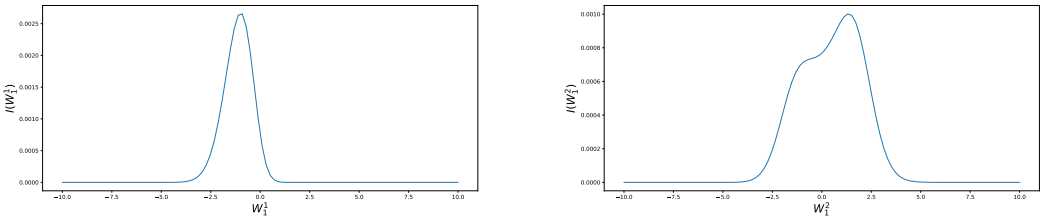

(a) (b)

Figure 2: Plotting the integrand I (in (8)) as a function of W_1 coordinates for $H = 0.07$ and $N = 2$.

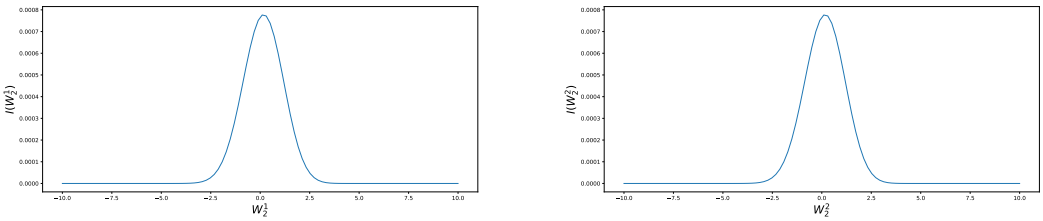

(a) (b)

Figure 3: Plotting the integrand I (in (8)) as a function of W_2 coordinates for $H = 0.07$ and $N = 2$.

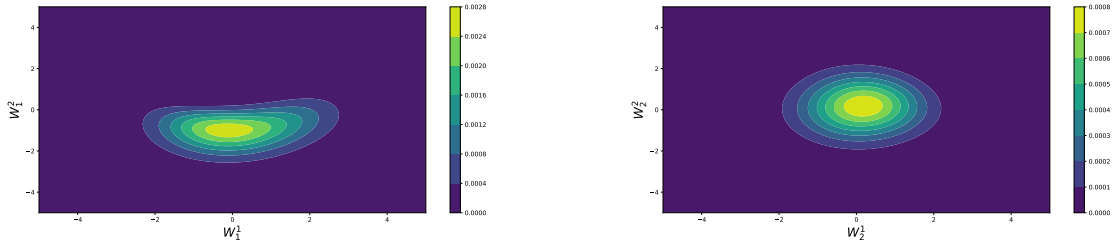

(a) (b)

Figure 4: Two dimensional Plotting of the integrand I (in (8)) for $H = 0.07$ and $N = 2$, a) function of W_1 coordinates, b) function of W_2 coordinates

6.1.2 N=4, H=0.07

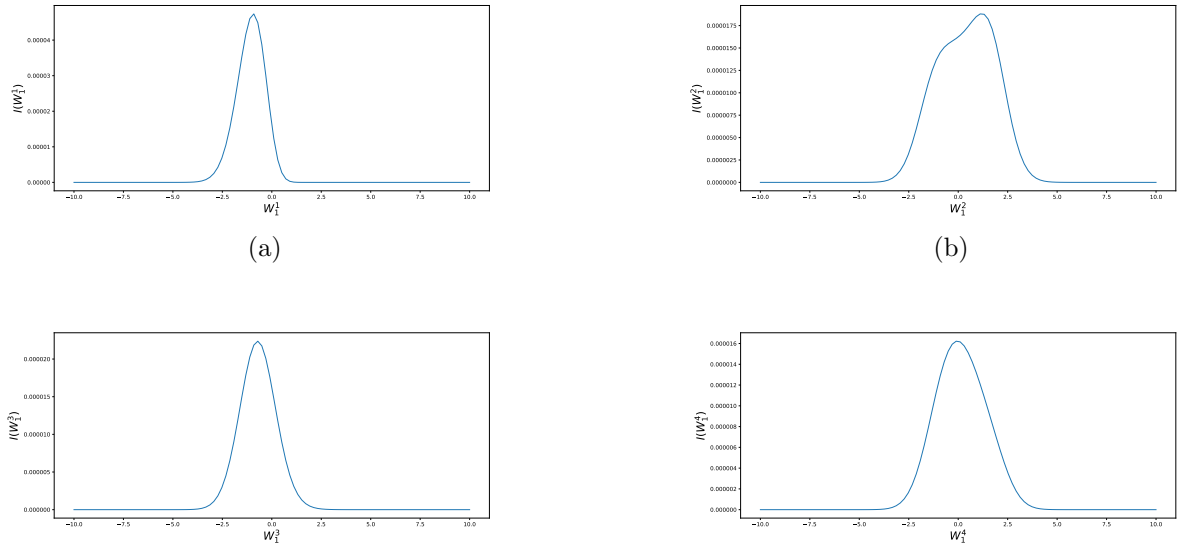

(a) (b)

(c) (d)

Figure 5: Plotting the integrand I (in (8)) as a function of W_1 coordinates for $H = 0.07$ and $N = 4$.

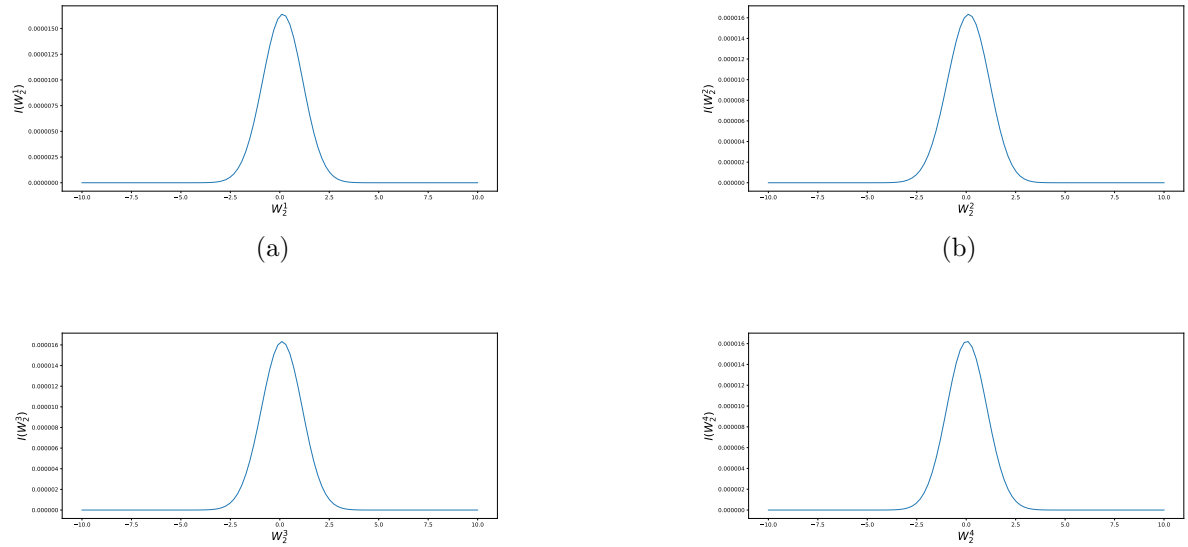

(a) (b)

(c) (d)

Figure 6: Plotting the integrand I (in (8)) as a function of W_2 coordinates for $H = 0.07$ and $N = 4$.

6.2 Comparing the mixed differences rates

In this section, we compare the mixed differences rates for the standard case against the case where we do a partial change of measure wrt W_1 coordinates (see Appendix A), for the case of $N = 4$ time steps. From the plots, we may notice that we face a bad behavior for the second differences,

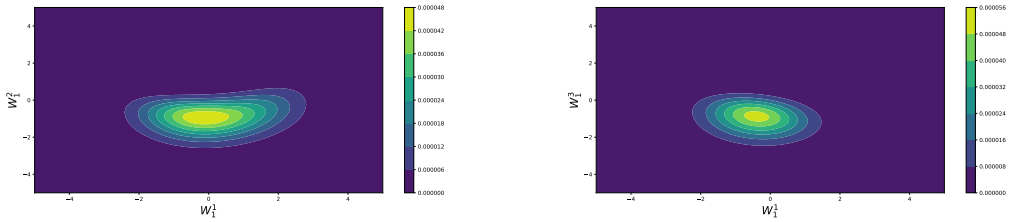

(a) (b)

Figure 7: Two dimensional Plotting of the integrand I (in (8)) for $H = 0.07$ and $N = 4$, a) function of W_1^1 and W_1^2 , b) function of W_1^1 and W_1^3

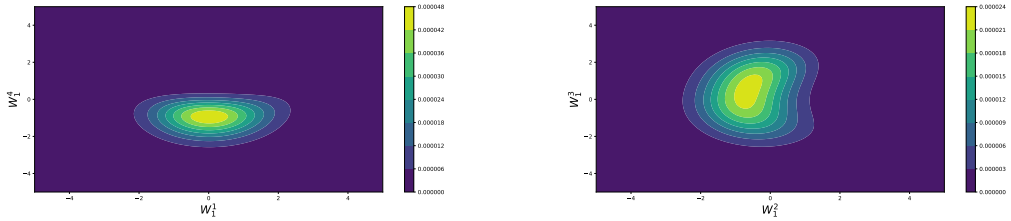

(a) (b)

Figure 8: Two dimensional Plotting of the integrand I (in (8)) for $H = 0.07$ and $N = 4$, a) function of W_1^1 and W_1^4 , b) function of W_1^2 and W_1^3

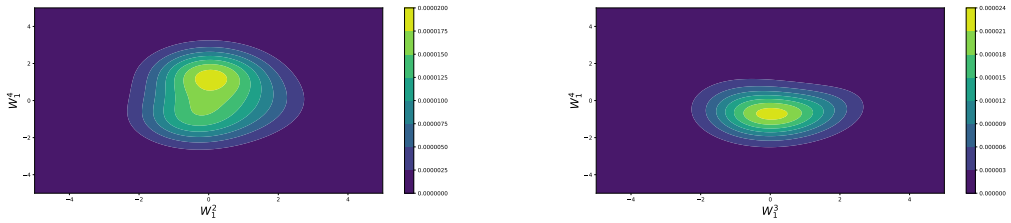

(a) (b)

Figure 9: Two dimensional Plotting of the integrand I (in (8)) for $H = 0.07$ and $N = 4$, a) function of W_1^2 and W_1^4 , b) function of W_1^3 and W_1^4

for the case without change of measure, which may explain the poor performance observed for MISC.This bad behavior is resolved when doing the partial change of measure. We obtained better results when using a measure change based on spectral decomposition rather than Cholesky decomposition. therefore by doing the change of measure, we obtained a more robust MISC solver.

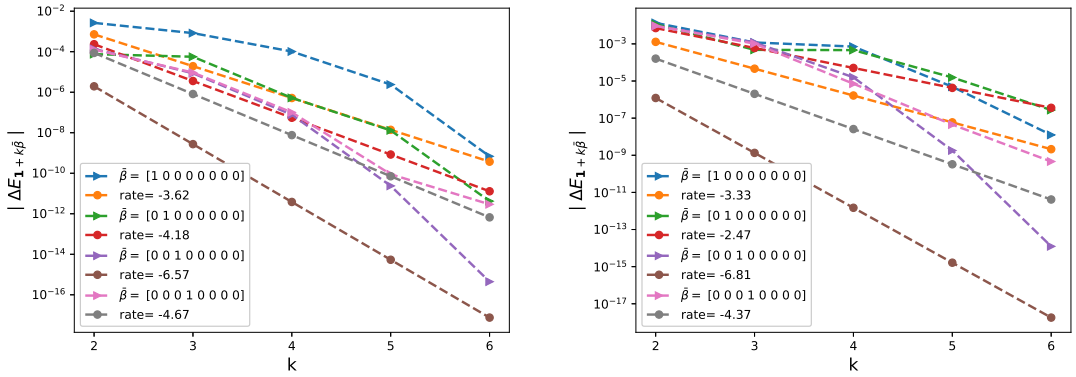

(a) (b)

Figure 10: The rate of convergence of first order differences $|\Delta E_\beta|$ $(\beta = \mathbf{1}+k\bar{\beta}))$, for W_1, for $K = 1$, $H = 0.07$: a) Without measure change b) With measure change

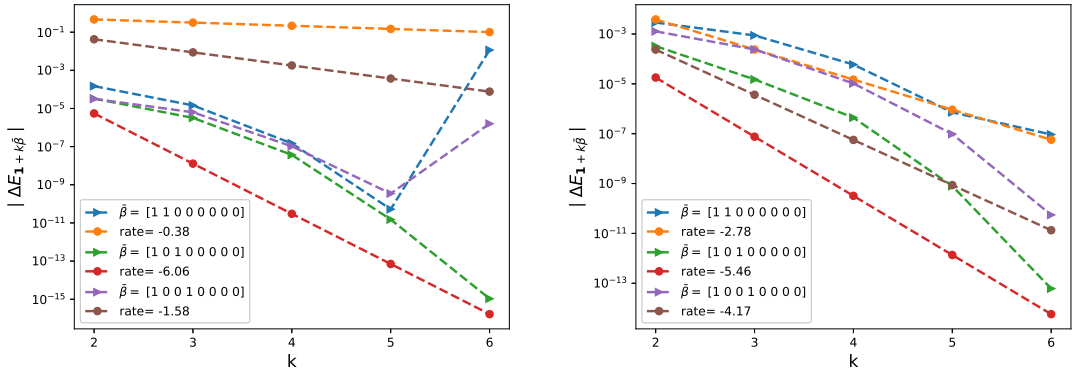

(a) (b)

Figure 11: The rate of convergence of second order differences $|\Delta E_\beta|$ $(\beta = \mathbf{1} + k\bar{\beta}))$, for W_1, for $K = 1$, $H = 0.07$: a) Without measure change b) With measure change

6.3 Weak error plots

In this section, I include the results of weak error rates for both cases: without and with change of meausure and without and with Richardson extrapolation, for $H \in \{0.43, 0.07\}$. The reference solution was computed with $N = 500$ time steps. We note that for the case where we do a partial chnage of measure, we limit the maximum number of changed coordinates up to 4, due to practical purposes related to the optimization procedure.

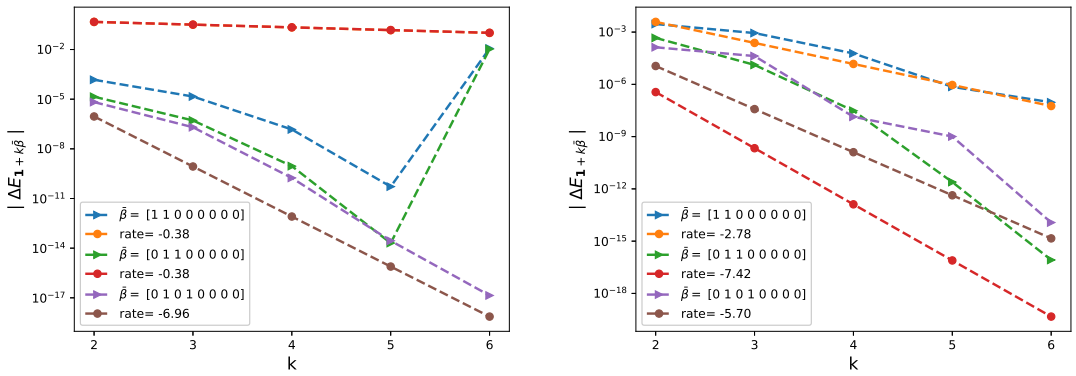

(a) (b)

Figure 12: The rate of convergence of second order differences $|\Delta E_\beta|$ $(\beta = \mathbf{1} + k\bar{\beta})$, for W_1, for $K = 1$, $H = 0.07$: a) Without measure change b) With measure change

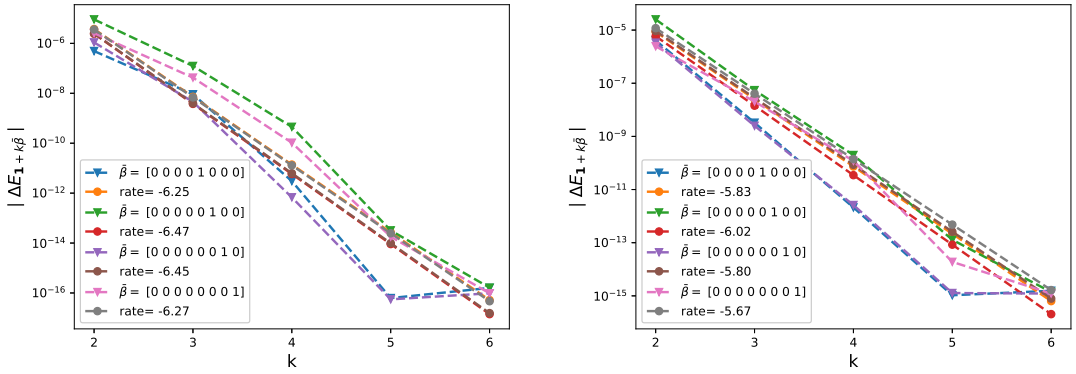

(a) (b)

Figure 13: The rate of convergence of first order differences $|\Delta E_\beta|$ $(\beta = \mathbf{1}+k\bar{\beta})$, for W_2, for $K = 1$, $H = 0.07$: a) Without measure change b) With measure change

6.3.1 Without change of measure

Without Richardson extrapolation

From figures (15 and 16), we see that for both cases $H \in \{0.43, 0.07\}$, we get a weak error of order Δt. The upper and lower bounds are 95% confidence interval.

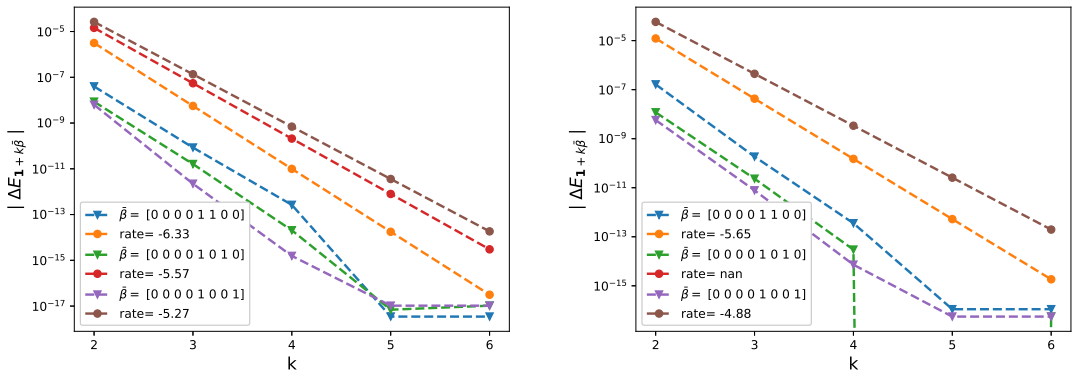

(a) (b)

Figure 14: The rate of convergence of second order differences $|\Delta E_\beta|$ $(\beta = \mathbf{1} + k\bar{\beta})$), for W_2, for $K = 1$, $H = 0.07$: a) Without measure change b) With measure change

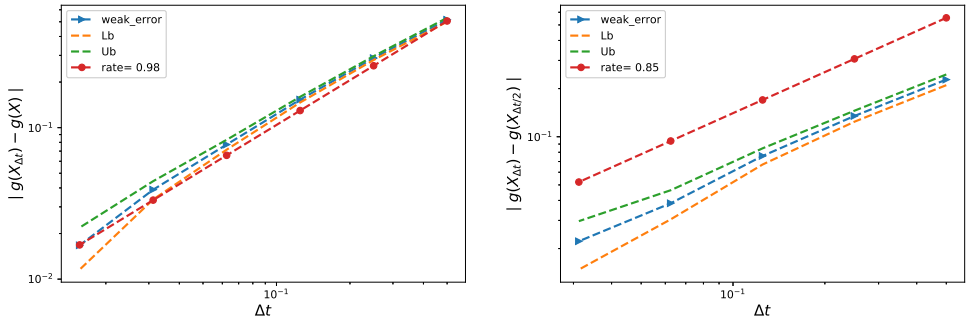

(a) (b)

Figure 15: The rate of convergence of the weak error for $H = 0.43$ $K = 1$, without Richardson extraploation, using MC with $M = 10^5$: a) $|\mathrm{E}\left[g(X_{\Delta t})\right] - g(X)|$ b) $\left|\mathrm{E}\left[g(X_{\Delta t}) - g(X_{\Delta t/2})\right]\right|$

With Richardson extrapolation (level 1)

From figures (17 and 18), we see that for both cases $H \in \{0.43, 0.07\}$, we get a weak error of order Δt^2 (We can see this from the first points, however I think the last points are influenced by the statistical error). The upper and lower bounds are 95% confidence interval.

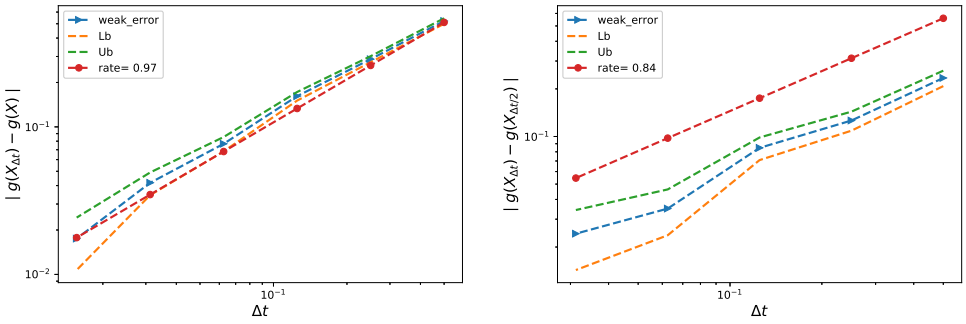

(a) (b)

Figure 16: The rate of convergence of the weak error for $H = 0.07$ $K = 1$, without Richardson extraploation, using MC with $M = 10^5$: a) $|\mathrm{E}\left[g(X_{\Delta t})\right] - g(X)|$ b) $\left|\mathrm{E}\left[g(X_{\Delta t}) - g(X_{\Delta t/2})\right]\right|$

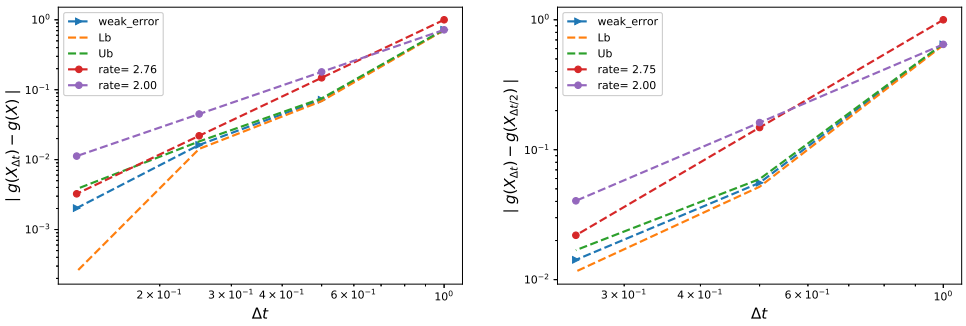

(a) (b)

Figure 17: The rate of convergence of the weak error for $H = 0.43$ $K = 1$, with Richardson extraploation, using MC with $M = 10^6$: a) $\left|\mathrm{E}\left[2g(X_{\Delta t/2}) - g(X_{\Delta t})\right] - g(X)\right|$ b) $\left|\mathrm{E}\left[3g(X_{\Delta t/2}) - g(X_{\Delta t}) - 2g(X_{\Delta t/4})\right]\right|$

With Richardson extrapolation (level 2)

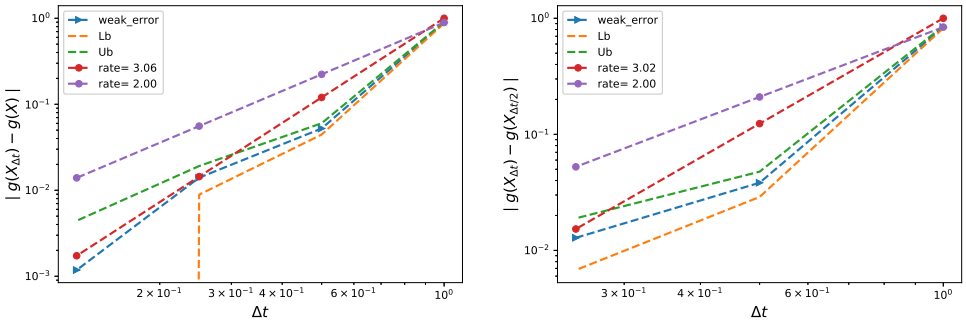

(a) (b)

Figure 18: The rate of convergence of the weak error for $H = 0.07$ $K = 1$, with Richardson extraploation, using MC with $M = 10^6$: a) $\left|\mathrm{E}\left[2g(X_{\Delta t/2}) - g(X_{\Delta t})\right] - g(X)\right|$ b) $\left|\mathrm{E}\left[3g(X_{\Delta t/2}) - g(X_{\Delta t}) - 2g(X_{\Delta t/4})\right]\right|$

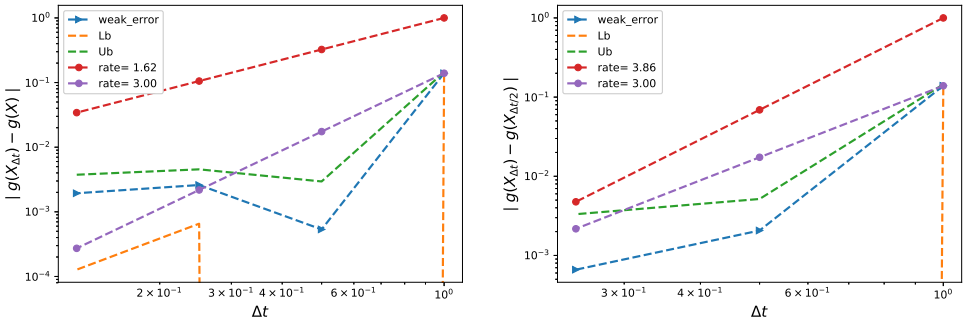

(a) (b)

Figure 19: The rate of convergence of the weak error for $H = 0.43$ $K = 1$, with Richardson extraploation, using MC with $M = 10^6$: a) $\left|\frac{1}{3}\mathrm{E}\left[8g(X_{\Delta t/4}) - 6g(X_{\Delta t/2}) + g(X_{\Delta t})\right] - g(X)\right|$ b) $\left|\frac{1}{3}\mathrm{E}\left[-8g(X_{\Delta t/8}) + 14g(X_{\Delta t/4}) - 7(X_{\Delta t/2}) + g(X_{\Delta t})\right]\right|$

6.3.2 With change of measure

Without Richardson extrapolation

From figures 16), we see that for $H = 0.07$, we get a weak error of order Δt. The upper and lower bounds are 95% confidence interval.

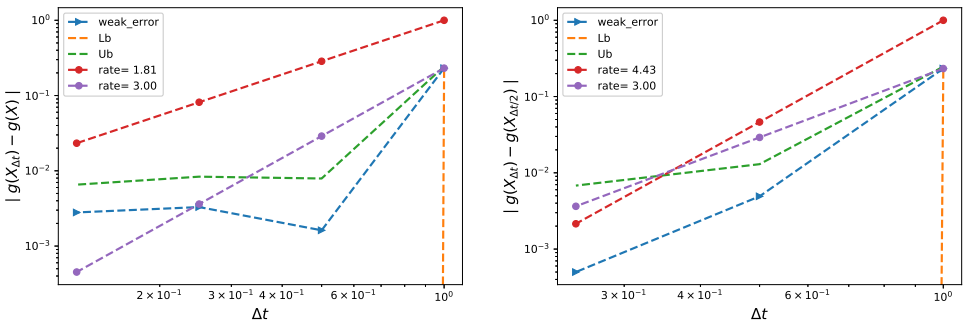

(a) (b)

Figure 20: The rate of convergence of the weak error for $H = 0.07$ $K = 1$, with Richardson extraploation (level 2), using MC with $M = 10^6$: a) $\left|\frac{1}{3}\mathrm{E}\left[8g(X_{\Delta t/4}) - 6g(X_{\Delta t/2}) + g(X_{\Delta t})\right] - g(X)\right|$ b) $\left|\frac{1}{3}\mathrm{E}\left[-8g(X_{\Delta t/8}) + 14g(X_{\Delta t/4}) - 7(X_{\Delta t/2}) + g(X_{\Delta t})\right]\right|$

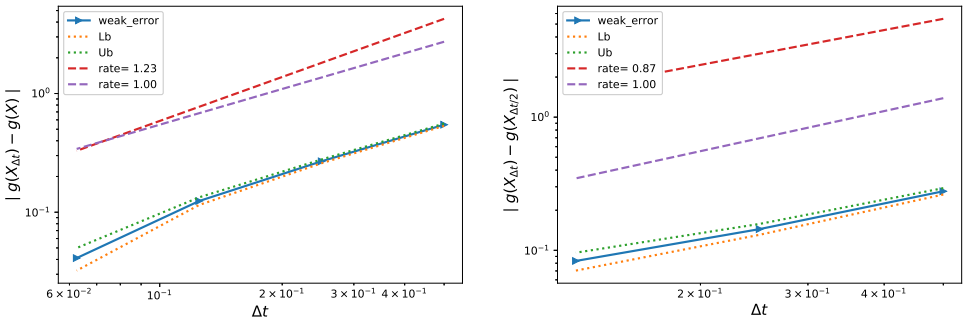

(a) (b)

Figure 21: The rate of convergence of the weak error for $H = 0.07$ $K = 1$, without Richardson extraploation, using MC with $M = 10^5$: a) $|\mathrm{E}\left[g(X_{\Delta t})\right] - g(X)|$ b) $\left|\mathrm{E}\left[g(X_{\Delta t}) - g(X_{\Delta t/2})\right]\right|$

6.4 Comparing relative errors using hierarchical representation

The used parameters are $H = \{0.43, 0.07\}$, $\eta = 1.9$, $\rho = -0.9$, $T = 1, K = 1$ and $\xi_0 = 0.235^2$. The results were reported for number of time steps $N \in \{2, 4, 8, 16\}$. Also, we use $S_0 = 1$, so the options will be prices in terms of the moneyness K, where K is the strike price.

In the following, we compare the relative errors for H $\in \{0.43, 0.07\}$ (see appendices B.3 and B.4 for the values of Call option prices). We note that for each case the reference solution was computed for $N = 500$ (number of time steps) using MC with 10^6 samples. In each case we report the results for 3 scenarios: i) Without using Richardson extrapolation, ii) Using level 1 Richardson extrapoaltion and iii) Using level 2 Richardson extrapoaltion. Tables (1, 2, 3) coresspond to $H = 0.43$ and tables (4, 5, 6) coresspond to $H = 0.07$.

Given the normalized bias computed by MC method (See Section 6.3) (reported as bold values in the tables), we report in red in each table the smallest tolerance that MISC required to get below

that relative bias (I do not put values for smaller tolerances, once the required bias is reached).

From the tables below, we have the following observations:

- Using Richardson extrapoaltion, we got a significant improvement for the relative error with the use of minimal time steps. For instance, for $H = 0.43$, we achieved around 8% of relative error, with 16 time steps when not using Richardson extrapolation (see table 1). However, When using level 1 of Richardson extrapolation (see table 2), we achieved around 6% of relative error, with only 2 time steps in the coarse level, and we got around 1% of relative error, with 4 time steps in the coarse level. A more significant improvement is seen with level 2 of Richardson extrapolation, in fact, with just 1 step in the coarse level, we got around 3% percent of relative error.

- For $H = 0.07$, we achieved around 8% of relative error, with 16 time steps when not using Richardson extrapolation (see table 4). However, When using level 1 of Richardson extrapolation (see table 5), we achieved around 5% of relative error, with only 2 time steps in the coarse level, and we got below 1% of relative error, with 4 time steps in the coarse level. We observed a less significant improvement when using levle 2 of Ricchardson extrapolation, compared to the case of $H = 0.43$.

6.4.1 Case $H = 0.43$, Relative error for different methods

Method \Steps	2	4	8	16
MISC ($TOl = 5.10^{-1}$)	0.6011	0.3497	0.1910	0.0969
MISC ($TOl = 2.10^{-1}$)	0.6011	0.3497	0.1910	0.0801
MISC ($TOl = 10^{-1}$)	0.6011	0.3497	0.2233	0.1236
MISC ($TOl = 5.10^{-2}$)	0.6011	0.3539	0.1882	0.1573
MISC ($TOl = 10^{-2}$)	0.5126	0.3258	0.1770	0.0829
MISC ($TOl = 5.10^{-3}$)	0.4930	0.3076	0.1671	–
MISC ($TOl = 10^{-3}$)	0.5126	0.2935	0.1503	–
MISC ($TOl = 10^{-4}$)	0.5154	0.2935	–	–
MC method ($M = 10^6$)	**0.5154**	**0.2935**	**0.1545**	**0.0801**

Table 1: Relative error of Call option price of the different tolerances for different number of time steps. Case $K = 1$, $H = 0.43$, without Richardson extrapolation

Method \Steps	$1-2$	$2-4$	$4-8$	$8-16$
MISC ($TOl = 5.10^{-1}$)	0.9059	0.0997	0.0323	0.0028
MISC ($TOl = 10^{-1}$)	0.9059	0.0997	0.1025	0.0688
MISC ($TOl = 5.10^{-2}$)	0.9059	0.1671	0.0857	0.0646
MISC ($TOl = 10^{-2}$)	0.7374	0.0969	0.0463	0.0028
MISC ($TOl = 5.10^{-3}$)	0.7205	0.0941	0.0211	–
MISC ($TOl = 10^{-3}$)	0.7191	0.0758	0.0112	–
MISC ($TOl = 5.10^{-4}$)	0.7129	0.0609	–	–
MC method ($M = 10^6$)	**0.7133**	**0.0698**	**0.0160**	**0.0035**

Table 2: Relative error of Call option price of the different tolerances for different number of time steps. Case $K = 1$, $H = 0.43$, using Richardson extrapolation (level 1)

Method \Steps	$1-2-4$	$2-4-8$	$4-8-16$
MISC ($TOl = 5.10^{-1}$)	0.1699	0.0098	0.0056
MISC ($TOl = 2.10^{-1}$)	0.1699	–	0.0014
MISC ($TOl = 10^{-1}$)	0.2037	–	–
MISC ($TOl = 5.10^{-2}$)	0.0295	–	–
MC method ($M = 10^6$)	**0.1440**	**0.0180**	**0.0023**

Table 3: Relative error of Call option price of the different tolerances for different number of time steps. Case $K = 1$, $H = 0.43$, using Richardson extrapolation (level 2)

6.4.2 Case $H = 0.07$, Relative error for different methods

Method \Steps	2	4	8	16
MISC ($TOl = 5.10^{-1}$)	0.3662	0.1578	0.1010	0.0758
MISC ($TOl = 10^{-1}$)	0.3662	0.1578	–	–
MISC ($TOl = 5.10^{-2}$)	0.3662	–	–	–
MISC ($TOl = 10^{-2}$)	–	–	–	–
MC method ($M = 10^6$)	**0.5354**	**0.2879**	**0.1515**	**0.0783**

Table 4: Relative error of Call option price of the different tolerances for different number of time steps. Case $K = 1$, $H = 0.07$, without Richardson extrapolation

Method \Steps	$1-2$	$2-4$	$4-8$	$8-16$
MISC ($TOl = 5.10^{-1}$)	0.5682	0.0505	0.1389	0.1604
MISC ($TOl = 16.10^{-2}$)	0.5682	0.0505	0.1389	0.0038
MISC ($TOl = 10^{-1}$)	0.5682	0.0505	0.1692	–
MISC ($TOl = 5.10^{-2}$)	0.5682	0.1465	0.0088	–
MISC ($TOl = 10^{-2}$)	–	0.0669	0.0088	–
MC method ($M = 10^6$)	**0.8915**	**0.0537**	**0.0129**	**0.0043**

Table 5: Relative error of Call option price of the different tolerances for different number of time steps. Case $K = 1$, $H = 0.07$, using Richardson extrapolation (level 1)

Method \Steps	$1-2-4$	$2-4-8$	$4-8-16$
MISC ($TOl = 5.10^{-1}$)	0.2563	0.1692	0.1679
MISC ($TOl = 10^{-1}$)	0.2563	0.1566	0.0025
MISC ($TOl = 7.10^{-2}$)	0.3005	0.0227	–
MISC ($TOl = 5.10^{-2}$)	0.4874	–	–
MISC ($TOl = 10^{-2}$)	0.1742	–	–
MC method ($M = 10^6$)	**0.2231**	**0.0279**	**0.0035**

Table 6: Relative error of Call option price of the different tolerances for different number of time steps. Case $K = 1$, $H = 0.07$, using Richardson extrapolation (level 2)

References Cited

[1] Pierre Bajgrowicz, Olivier Scaillet, and Adrien Treccani. Jumps in high-frequency data: Spurious detections, dynamics, and news. *Management Science*, 62(8):2198–2217, 2015.

[2] Christian Bayer, Peter Friz, and Jim Gatheral. Pricing under rough volatility. *Quantitative Finance*, 16(6):887–904, 2016.

[3] Christian Bayer, Peter K Friz, Paul Gassiat, Joerg Martin, and Benjamin Stemper. A regularity structure for rough volatility. *arXiv preprint arXiv:1710.07481*, 2017.

[4] Christian Bayer, Peter K Friz, Archil Gulisashvili, Blanka Horvath, and Benjamin Stemper. Short-time near-the-money skew in rough fractional volatility models. *arXiv preprint arXiv:1703.05132*, 2017.

[5] Mikkel Bennedsen, Asger Lunde, and Mikko S Pakkanen. Decoupling the short-and long-term behavior of stochastic volatility. *arXiv preprint arXiv:1610.00332*, 2016.

[6] Mikkel Bennedsen, Asger Lunde, and Mikko S Pakkanen. Hybrid scheme for brownian semistationary processes. *Finance and Stochastics*, 21(4):931–965, 2017.

[7] F. Biagini, Y. Hu, B. Øksendal, and T. Zhang. *Stochastic Calculus for Fractional Brownian Motion and Applications*. Probability and Its Applications. Springer London, 2008.

[8] R. Carmona and M.R. Tehranchi. *Interest Rate Models: an Infinite Dimensional Stochastic Analysis Perspective*. Springer Finance. Springer Berlin Heidelberg, 2007.

[9] Kim Christensen, Roel CA Oomen, and Mark Podolskij. Fact or friction: Jumps at ultra high frequency. *Journal of Financial Economics*, 114(3):576–599, 2014.

[10] Laure Coutin. An introduction to (stochastic) calculus with respect to fractional brownian motion. In *Séminaire de Probabilités XL*, pages 3–65. Springer, 2007.

[11] Omar El Euch and Mathieu Rosenbaum. The characteristic function of rough heston models. *Mathematical Finance*, 2016.

[12] Martin Forde and Hongzhong Zhang. Asymptotics for rough stochastic volatility models. *SIAM Journal on Financial Mathematics*, 8(1):114–145, 2017.

[13] Jim Gatheral. *The volatility surface: a practitioner's guide*, volume 357. John Wiley & Sons, 2011.

[14] Jim Gatheral, Thibault Jaisson, Andrew Lesniewski, and Mathieu Rosenbaum. Volatility is rough, part 2: Pricing.

[15] Jim Gatheral, Thibault Jaisson, and Mathieu Rosenbaum. Volatility is rough. *arXiv preprint arXiv:1410.3394*, 2014.

[16] Blanka Horvath, Antoine Jacquier, and Aitor Muguruza. Functional central limit theorems for rough volatility. 2017.

[17] Antoine Jacquier, Claude Martini, and Aitor Muguruza. On vix futures in the rough bergomi model. *Quantitative Finance*, 18(1):45–61, 2018.

[18] Antoine Jacquier, Mikko S Pakkanen, and Henry Stone. Pathwise large deviations for the rough bergomi model. *arXiv preprint arXiv:1706.05291*, 2017.

[19] Benoit B Mandelbrot and John W Van Ness. Fractional brownian motions, fractional noises and applications. *SIAM review*, 10(4):422–437, 1968.

[20] Tina Marquardt et al. Fractional lévy processes with an application to long memory moving average processes. *Bernoulli*, 12(6):1099–1126, 2006.

[21] Ryan McCrickerd and Mikko S Pakkanen. Turbocharging monte carlo pricing for the rough bergomi model. *arXiv preprint arXiv:1708.02563*, 2017.

[22] David Nualart. *The Malliavin calculus and related topics*, volume 1995. Springer, 2006.

[23] Marc Romano and Nizar Touzi. Contingent claims and market completeness in a stochastic volatility model. *Mathematical Finance*, 7(4):399–412, 1997.

[24] Peter Tankov. Pricing and hedging in exponential lévy models: review of recent results. In *Paris-Princeton Lectures on Mathematical Finance 2010*, pages 319–359. Springer, 2011.

A Gaussian Hermite Quadrature with importance sampling

Let us call the integrand that we feed to MISC by $I(W_1, W_2)$, then

$$C_{RB}(T,K) = \int_{\mathbb{R}_+^{2N}} I(\mathbf{W}_1, \mathbf{W}_2)\rho(\mathbf{W}_1)\rho(\mathbf{W}_2)d\mathbf{W}_1 d\mathbf{W}_2, \tag{11}$$

where N is the number of time steps. We can rewrite the previous expression as

$$C_{RB}(T,K) = \int_{\mathbb{R}_+^{2N}} \frac{I(\mathbf{W}_1, \mathbf{W}_2)\rho(\mathbf{W}_1)}{h(\mathbf{W}_1; \widehat{\mathbf{W}}_1, \Psi)} h(\mathbf{W}_1; \widehat{\mathbf{W}}_1, \Psi)\rho(\mathbf{W}_2)d\mathbf{W}_1 d\mathbf{W}_2, \tag{12}$$

where $h(\mathbf{W}_1; \widehat{\mathbf{W}}_1, \Psi)$ is a multivariate normal density with first and second order moments given by

$$\widehat{\mathbf{W}}_1 = \arg\max_{\mathbf{W}_1 \in \mathbb{R}^N} [\log I(\mathbf{W}_1; \mathbf{W}_2)] \tag{13}$$

$$\Psi = \left(-\frac{\partial^2 [\log I(\mathbf{W}_1; \mathbf{W}_2)]}{\partial \mathbf{W}_1^T \mathbf{W}_1} \right)^{-1}_{\mathbf{W}_1 = \widehat{\mathbf{W}}_1} \tag{14}$$

Let us define $\tilde{\mathbf{W}}_1$ as uncorrelated varaibles and the Cholesky factorization of Ψ is given by $\Psi = LL^T$, and $\overline{\mathbf{W}}_1 = \sqrt{2}L\tilde{\mathbf{W}}_1 + \widehat{\mathbf{W}}_1$ then Eq 12 becomes

(15)

$$C_{RB}(T,K) = = 2^{N/2}.|L| \int_{\mathbb{R}_+^{2N}} \left(I(\overline{\mathbf{W}}_1, \mathbf{W}_2) \exp(-\frac{1}{2}\overline{\mathbf{W}}_1^T \overline{\mathbf{W}}_1) \exp(\frac{1}{2}\tilde{\mathbf{W}}^T \tilde{\mathbf{W}}) \right) \rho(\tilde{\mathbf{W}}_1)\rho(\mathbf{W}_2) d\tilde{\mathbf{W}}_1 d\mathbf{W}_2$$

B additional results

B.1 Integrand plotting wrt different random inputs N=2, H=0.43

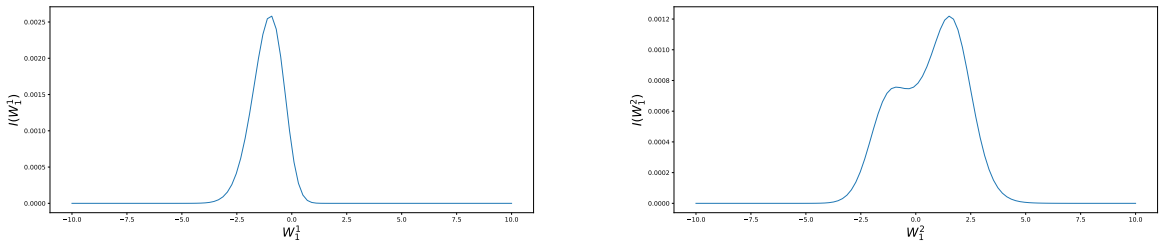

(a) (b)

Figure 22: Plotting the integrand I (in (8)) as a function of W_1 coordinates for $H = 0.43$ and $N = 2$.

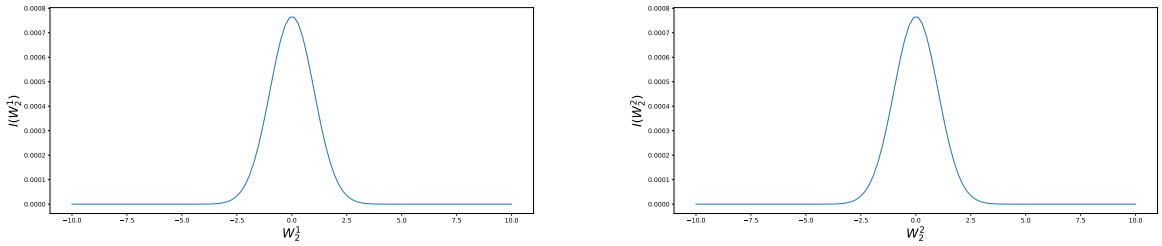

(a) (b)

Figure 23: Plotting the integrand I (in (8)) as a function of W_2 coordinates for $H = 0.43$ and $N = 2$.

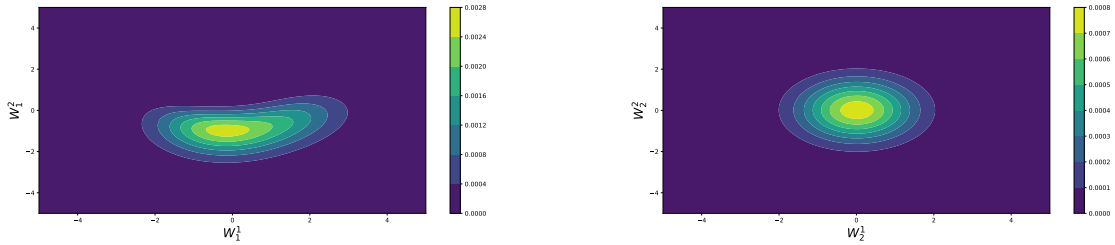

(a) (b)

Figure 24: Two dimensional Plotting of the integrand I (in (8)) for $H = 0.43$ and $N = 2$, a) function of W_1 coordinates, b) function of W_2 coordinates

B.2 Integrand plotting wrt different random inputs: N=4, H=0.43

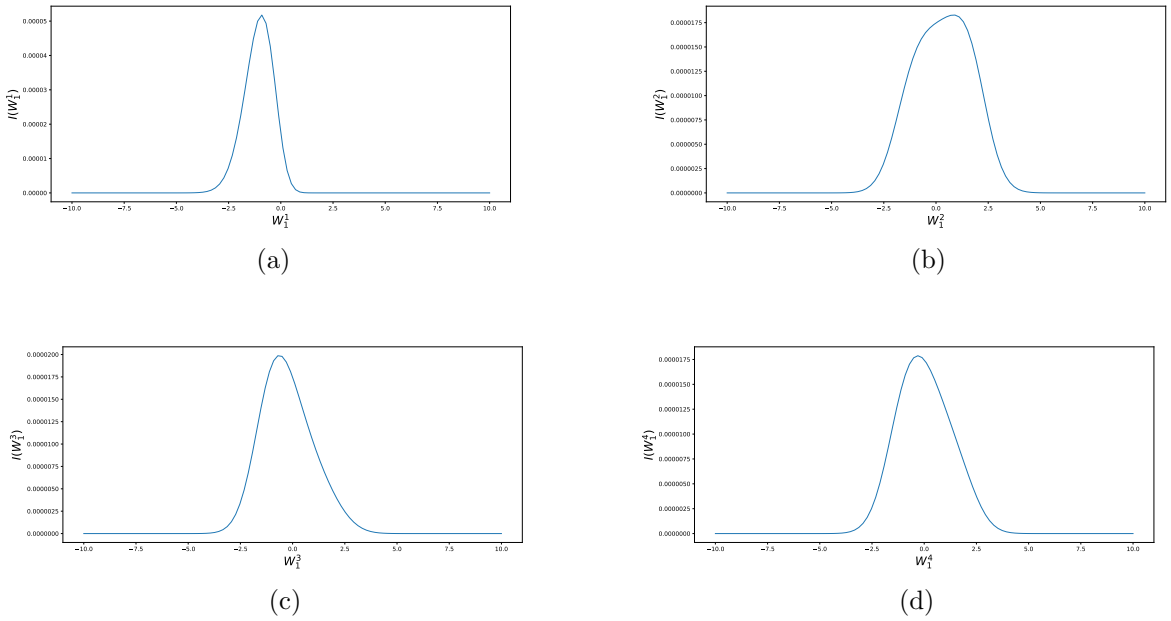

(a) (b)

(c) (d)

Figure 25: Plotting the integrand I (in (8)) as a function of W_1 coordinates for $H = 0.43$ and $N = 4$.

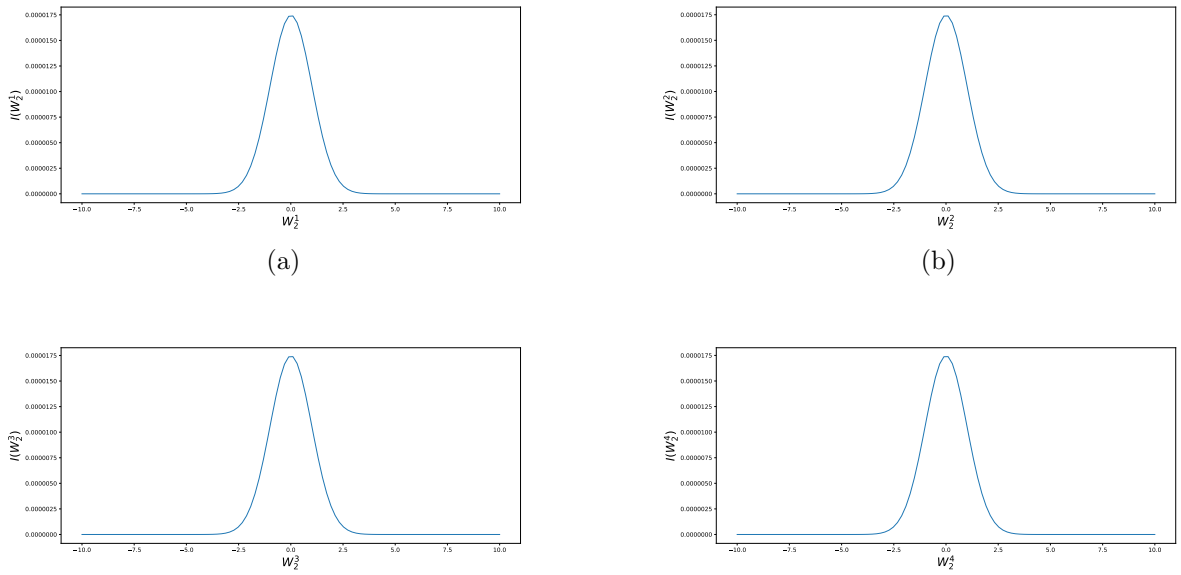

Figure 26: Plotting the integrand I (in (8)) as a function of W_2 coordinates for $H = 0.43$ and $N = 4$.

B.3 Case $H = 0.43$, Call prices for different methods

Method \Steps	2	4	8	16
MISC ($TOl = 5.10^{-1}$)	0.1140	0.0961	0.0848	0.0781
MISC ($TOl = 2.10^{-1}$)	0.1140	0.0961	0.0848	0.0769
MISC ($TOl = 10^{-1}$)	0.1140	0.0961	0.0871	0.0800
MISC ($TOl = 5.10^{-2}$)	0.1140	0.0964	0.0846	0.0824
MISC ($TOl = 10^{-2}$)	0.1077	0.0944	0.0838	0.0771
MISC ($TOl = 5.10^{-3}$)	0.1063	0.0931	0.0831	–
MISC ($TOl = 10^{-3}$)	0.1077	0.0921	0.0819	–
MISC ($TOl = 10^{-4}$)	0.1079	0.0921	–	–
MC method ($M = 10^6$)	0.1079 (1.55e−04)	0.0921 (9.65e−05)	0.0822 (7.61e−05)	0.0769 (6.65e−05)

Table 7: Call option price of the different methods for different number of time steps. Case $K = 1$, $H = 0.43$, without Richardson extrapolation. The values between parentheses in the tables are the standard errors for MC method

Method \Steps	$1-2$	$2-4$	$4-8$	$8-16$
MISC ($TOl = 5.10^{-1}$)	0.1357	0.0783	0.0735	0.0714
MISC ($TOl = 10^{-1}$)	0.1357	0.0783	0.0785	0.0761
MISC ($TOl = 5.10^{-2}$)	0.1357	0.0831	0.0773	0.0758
MISC ($TOl = 10^{-2}$)	0.1237	0.0781	0.0745	0.0714
MISC ($TOl = 5.10^{-3}$)	0.1225	0.0779	0.0727	–
MISC ($TOl = 10^{-3}$)	0.1224	0.0766	0.0720	–
MISC ($TOl = 5.10^{-4}$)	0.1221	0.0763	–	–

Table 8: Call option price of the different methods for different number of time steps. Case $K = 1$, $H = 0.43$, using Richardson extrapolation (level 1)

Method \Steps	$1-2-4$	$2-4-8$	$4-8-16$
MISC ($TOl = 5.10^{-1}$)	0.0591	0.0719	0.0708
MISC ($TOl = 2.10^{-1}$)	0.0591	–	0.0711
MISC ($TOl = 10^{-1}$)	0.0567	–	–
MISC ($TOl = 5.10^{-2}$)	0.0733	–	–

Table 9: Call option price of the different methods for different number of time steps. Case $K = 1$, $H = 0.43$, using Richardson extrapolation (level 2)

B.4 Case $H = 0.07$, Call prices for different methods

Method \Steps	2	4	8	16
MISC ($TOl = 5.10^{-1}$)	0.1082	0.0917	0.0872	0.0732
MISC ($TOl = 10^{-1}$)	0.1082	0.0917	–	–
MISC ($TOl = 5.10^{-2}$)	0.1082	–	–	–
MISC ($TOl = 10^{-2}$)	–	–	–	–
MC method ($M = 10^6$)	0.1216 (1.05e−03)	0.1020 (1.86e−04)	0.0912 (1.35e−04)	0.0854 (1.08e−04)

Table 10: Call option price of the different methods for different number of time steps. Case $K = 1$, without Richardson extrapolation. The values between parentheses in the tables are the standard errors for MC method

Method \Steps	$1-2$	$2-4$	$4-8$	$8-16$
MISC ($TOl = 5.10^{-1}$)	0.1242	0.0752	0.0682	0.0665
MISC ($TOl = 16.10^{-2}$)	0.1242	0.0752	0.0682	0.0795
MISC ($TOl = 10^{-1}$)	0.1242	0.0752	0.0658	–
MISC ($TOl = 5.10^{-2}$)	0.1242	0.0676	0.0799	–
MISC ($TOl = 10^{-2}$)	–	0.0845	0.0799	–

Table 11: Call option price of the different methods for different number of time steps. Case $K = 1$, $H = 0.07$, using Richardson extrapolation (level 1)

Method \Steps	$1-2-4$	$2-4-8$	$4-8-16$
MISC ($TOl = 5.10^{-1}$)	0.0589	0.0658	0.0659
MISC ($TOl = 10^{-1}$)	0.0589	0.0668	0.079
MISC ($TOl = 7.10^{-2}$)	0.0554	0.0810	–
MISC ($TOl = 5.10^{-2}$)	0.0406	–	–
MISC ($TOl = 10^{-2}$)	0.0654	–	–

Table 12: Call option price of the different methods for different number of time steps. Case $K = 1$, $H = 0.07$, using Richardson extrapolation (level 2)

B.5 Comparing call options prices

B.5.1 Without Hierarchical representation

Case $H = 0.43$

Method \Steps	2	4	8	16
MISC ($TOl = 5.10^{-1}$)	0.1057	0.0988	0.0944	0.0921
MISC ($TOl = 10^{-1}$)	0.1057	0.0988	0.0836	0.0594
MISC ($TOl = 5.10^{-2}$)	0.1057	0.0976	0.0758	0.0781
MISC ($TOl = 10^{-2}$)	0.1113	0.0940	0.0820	–
MC method ($M = 10^6$)	0.1079 (1.55e−04)	0.0921 (9.65e−05)	0.0822 (7.61e−05)	0.0769 (6.65e−05)

Table 13: Call option price of the different methods for different number of time steps. Case $K = 1$

Case $H = 0.07$

Method \Steps	2	4	8	16
MISC ($TOl = 5.10^{-1}$)	0.1065	0.0900	0.0809	0.0762
MISC ($TOl = 10^{-1}$)	0.1065	0.0900	0.0733	0.0956
MISC ($TOl = 5.10^{-2}$)	0.1065	0.0898	0.0881	–
MISC ($TOl = 10^{-2}$)	0.1226	0.1022	0.0933	–
MC method ($M = 10^6$)	0.1216 (1.05e−03)	0.1020 (1.86e−04)	0.0912 (1.35e−04)	0.0854 (1.08e−04)

Table 14: Call option price of the different methods for different number of time steps. Case $K = 1$

B.6 Investigating differences wrt H

B.6.1 Totally Hierarchical

In this section, we do both hierarchical transformation, based on brownian bridges, for both directions W_1 and W_2.

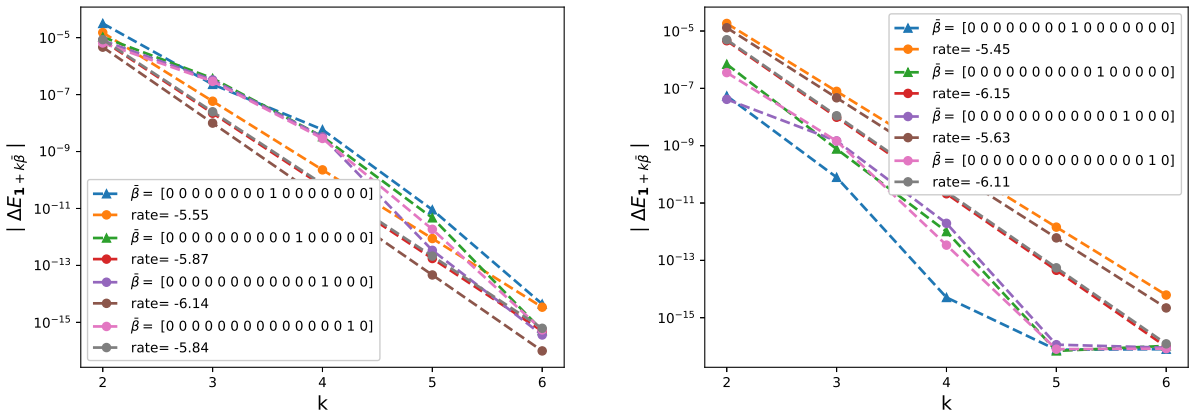

(a) (b)

Figure 27: The rate of convergence of first order differences $|\Delta E_\beta|$ $(\beta = \mathbf{1} + k\bar{\beta})$ for $K = 1$: a) Without hierarchical for W_2 b) With hierarchical for W_2

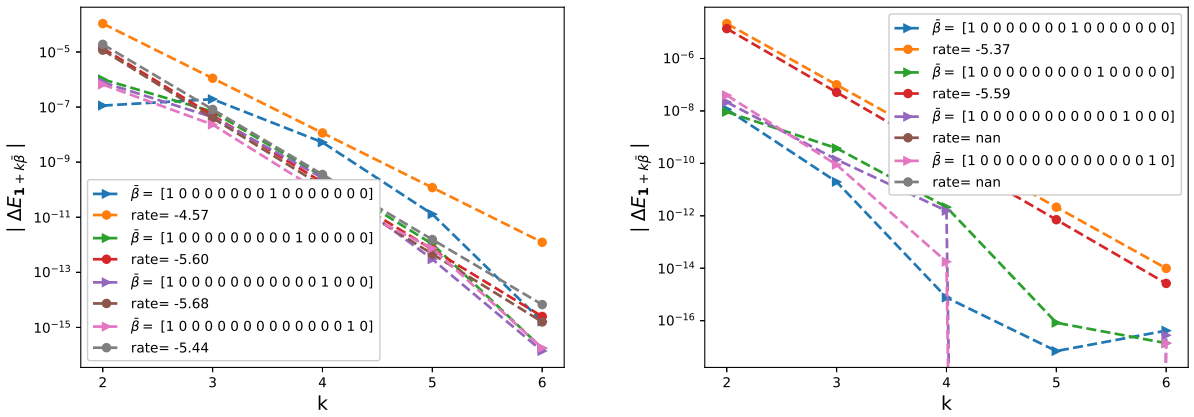

(a) (b)

Figure 28: The rate of convergence of mixed order differences $|\Delta E_\beta|$ $(\beta = \mathbf{1} + k\bar{\beta})$ for $K = 1$: a) Without hierarchical for W_2 b) With hierarchical for W_2

B.6.2 Hierarchical

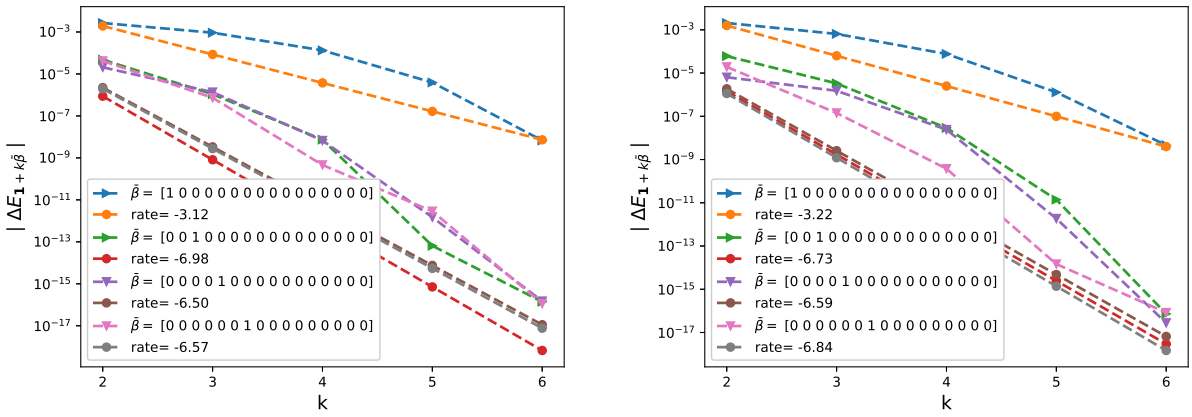

(a) (b)

Figure 29: The rate of convergence of first order differences $|\Delta E_\beta|$ $(\beta = \mathbf{1} + k\bar{\beta}))$ for $K = 1$: a) $H = 0.43$ b) $H = 0.07$

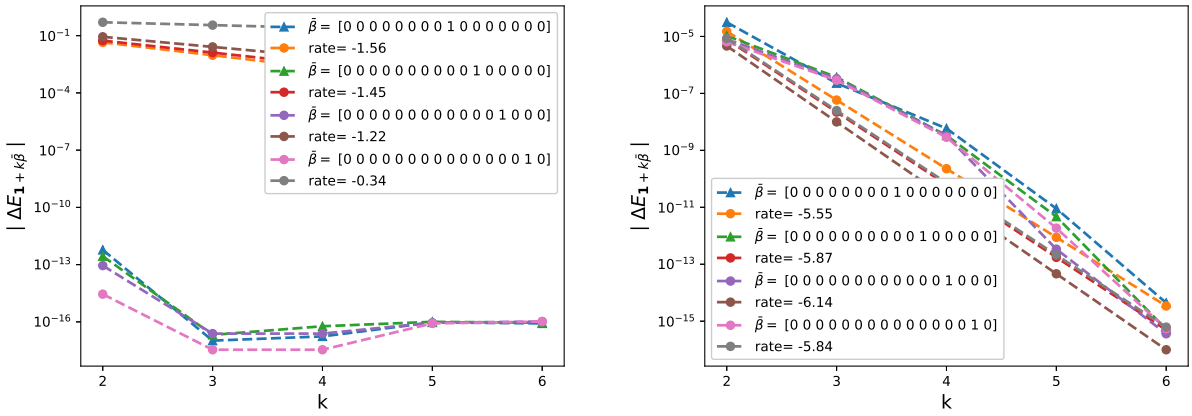

(a) (b)

Figure 30: The rate of convergence of first order differences $|\Delta E_\beta|$ $(\beta = \mathbf{1} + k\bar{\beta}))$ for $K = 1$: a) $H = 0.43$ b) $H = 0.07$

B.6.3 Non Hierarchical

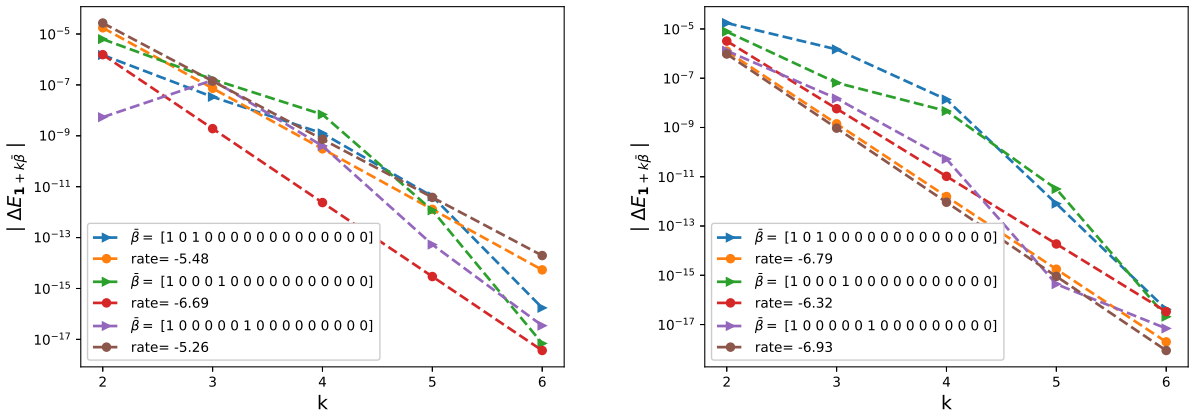

(a) (b)

Figure 31: The rate of convergence of mixed order differences $|\Delta E_\beta|$ $(\beta = \mathbf{1} + k\bar{\beta})$ for $K = 1$: a) $H = 0.43$ b) $H = 0.07$

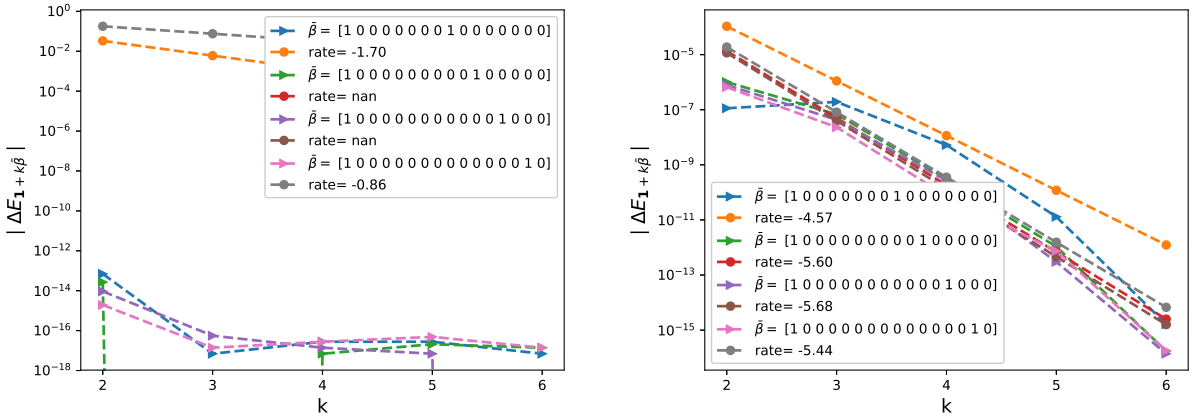

(a) (b)

Figure 32: The rate of convergence of mixed order differences $|\Delta E_\beta|$ $(\beta = \mathbf{1} + k\bar{\beta})$ for $K = 1$: a) $H = 0.43$ b) $H = 0.07$

B.7 Investigating mixed differences wrt ρ

N=4, K=1

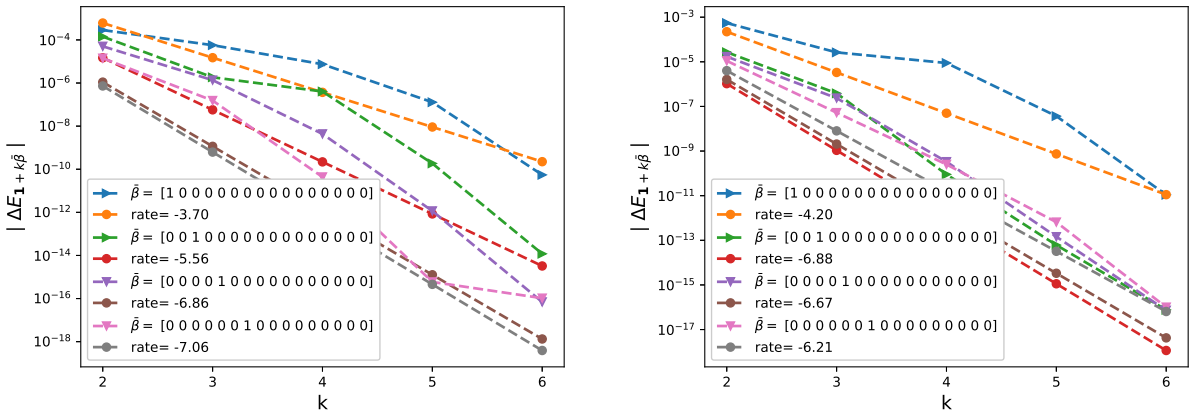

(a) (b)

Figure 33: The rate of convergence of first order differences $|\Delta E_\beta|$ $(\beta = \mathbf{1} + k\bar{\beta}))$ for $K = 1$: a) $H = 0.43$ b) $H = 0.07$

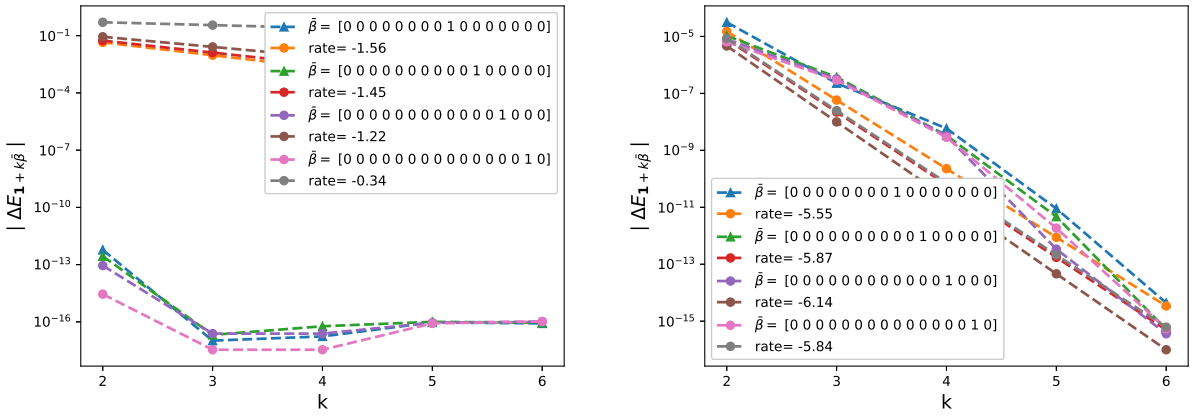

(a) (b)

Figure 34: The rate of convergence of first order differences $|\Delta E_\beta|$ $(\beta = \mathbf{1} + k\bar{\beta}))$ for $K = 1$: a) $H = 0.43$ b) $H = 0.07$

N=8, K=1

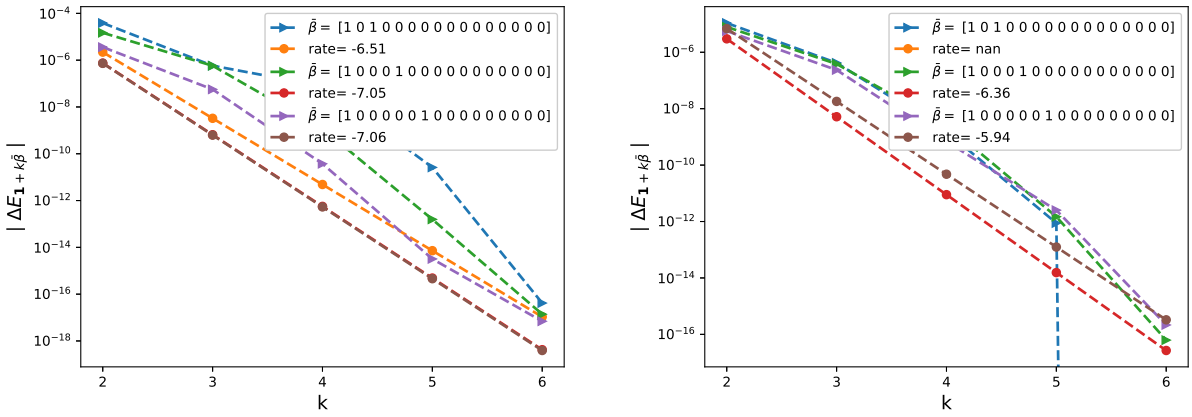

(a) (b)

Figure 35: The rate of convergence of mixed order differences $|\Delta E_\beta|$ $(\beta = \mathbf{1} + k\overline{\beta}))$ for $K = 1$: a) $H = 0.43$ b) $H = 0.07$

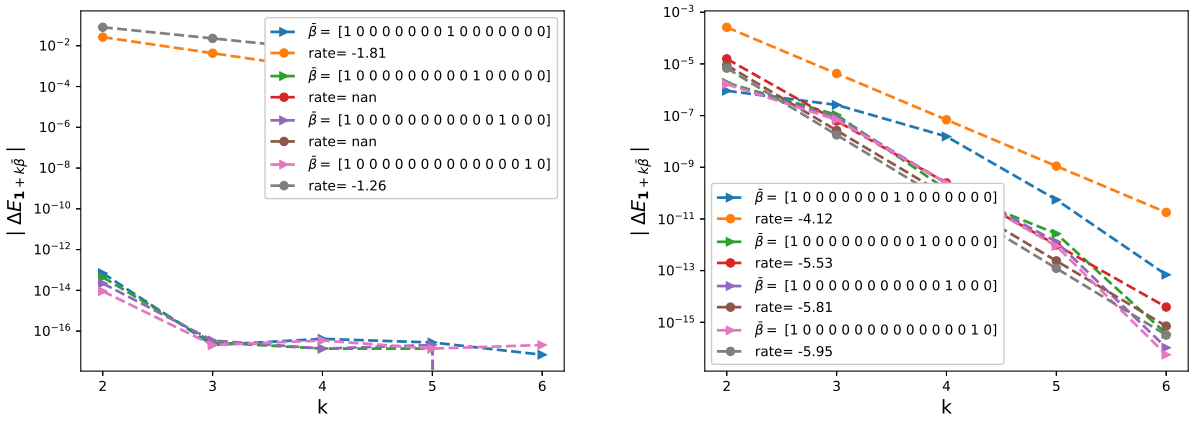

(a) (b)

Figure 36: The rate of convergence of mixed order differences $|\Delta E_\beta|$ $(\beta = \mathbf{1} + k\overline{\beta}))$ for $K = 1$: a) $H = 0.43$ b) $H = 0.07$

N=4, K=0.8

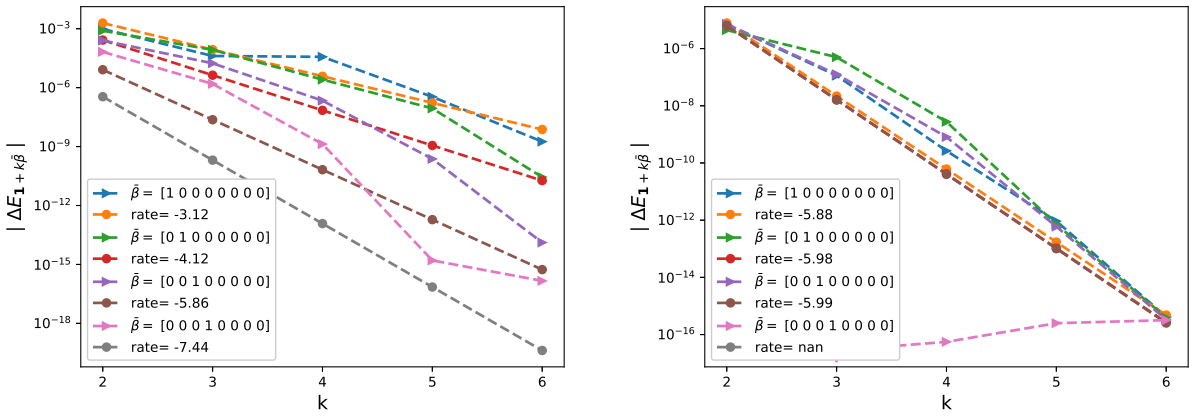

(a) (b)

Figure 37: The rate of convergence of first order differences $|\Delta E_\beta|$ $(\beta = \mathbf{1} + k\bar{\beta})$ for $K = 1$: a) $\rho = -0.9$ b) $\rho = 0$.

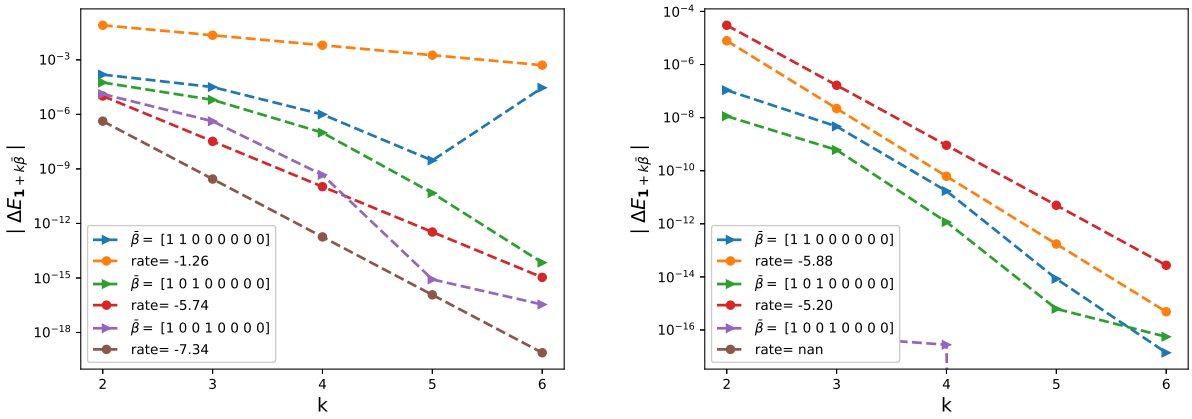

(a) (b)

Figure 38: The rate of convergence of mixed order differences $|\Delta E_\beta|$ $(\beta = \mathbf{1} + k\bar{\beta})$): a) $\rho = -0.9$ b) $\rho = 0$.

N=8, K=0.8

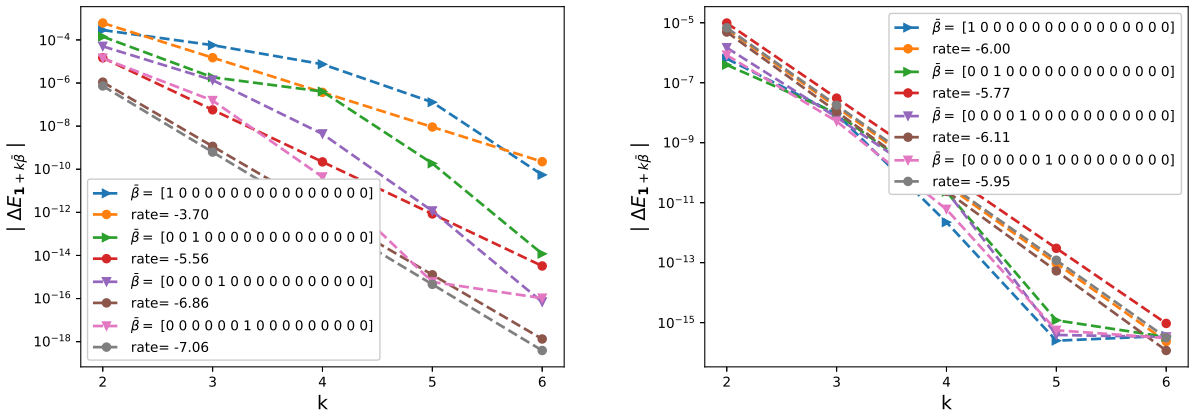

(a) (b)

Figure 39: The rate of convergence of first order differences $|\Delta E_\beta|$ $(\beta = \mathbf{1} + k\bar{\beta})$): a) $\rho = -0.9$ b) $\rho = 0$.

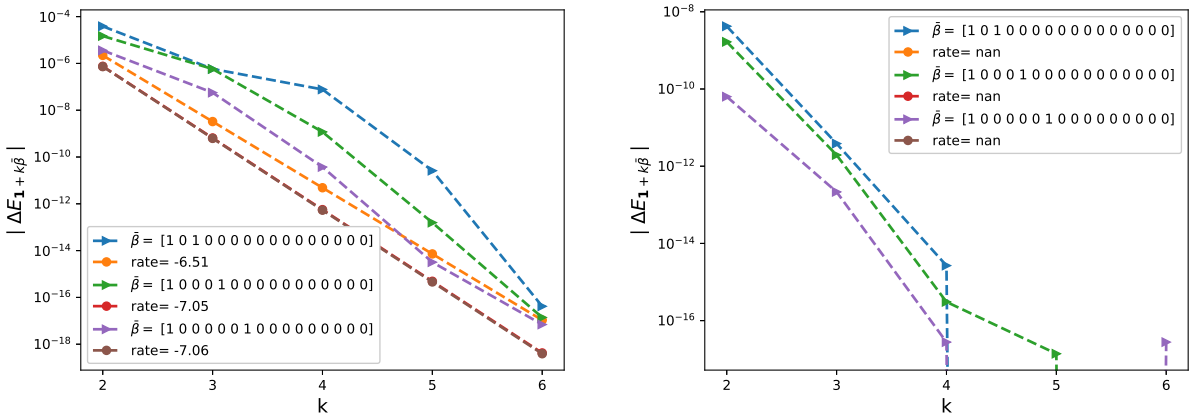

(a) (b)

Figure 40: The rate of convergence of mixed order differences $|\Delta E_\beta|$ $(\beta = \mathbf{1} + k\bar{\beta})$): a) $\rho = -0.9$ b) $\rho = 0$.

B.8 Investigating mixed differences wrt ξ

N=4, K=1

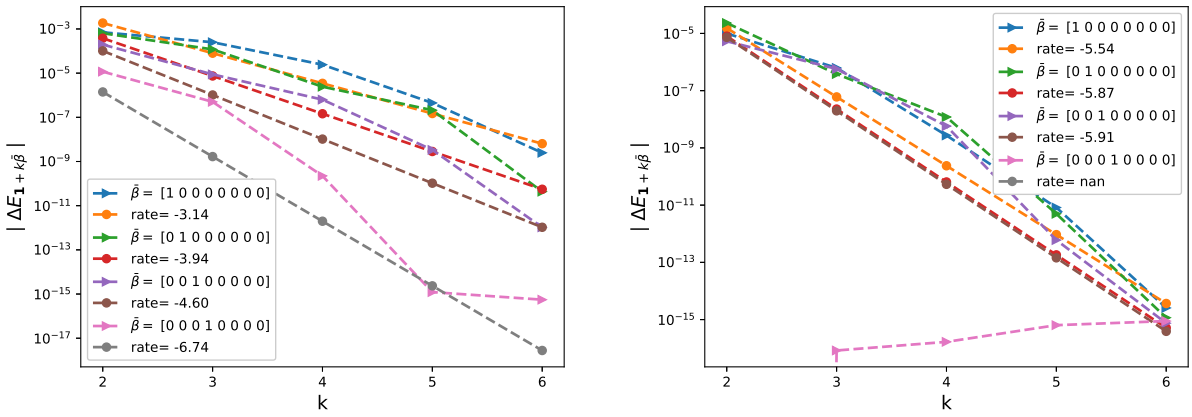

(a) (b)

Figure 41: The rate of convergence of first order differences $|\Delta E_\beta|$ ($\beta = \mathbf{1} + k\bar{\beta}$)): a) $\rho = -0.9$ b) $\rho = 0$.

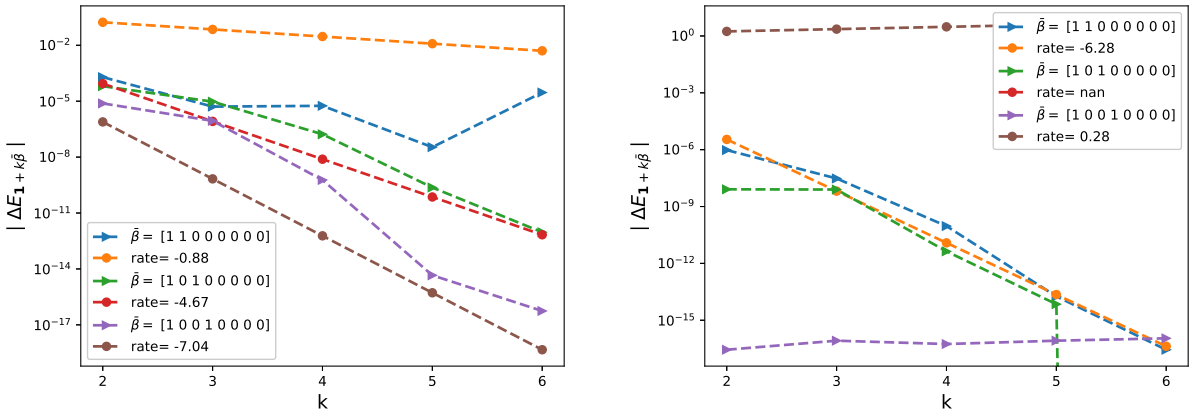

(a) (b)

Figure 42: The rate of convergence of mixed order differences $|\Delta E_\beta|$ ($\beta = \mathbf{1} + k\bar{\beta}$)): a) $\rho = -0.9$ b) $\rho = 0$.

N=8, K=1

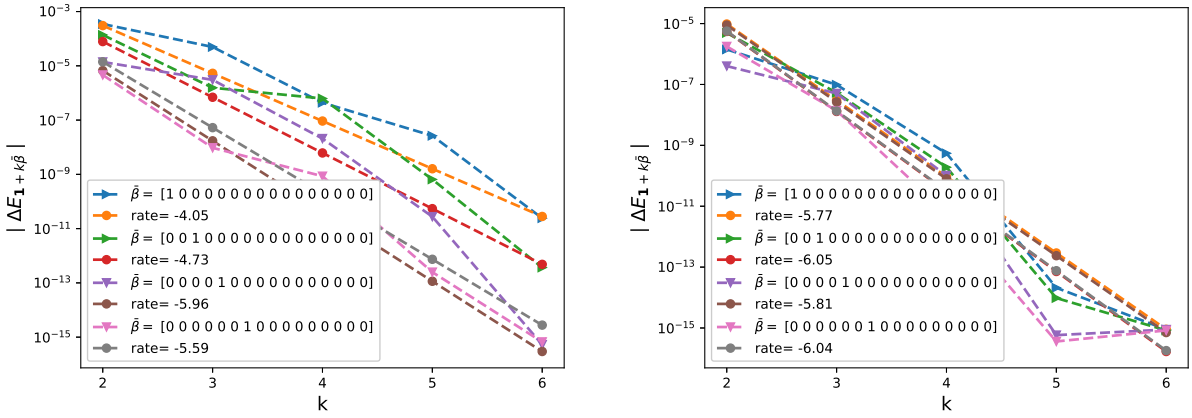

(a) (b)

Figure 43: The rate of convergence of first order differences $|\Delta E_\beta|$ $(\beta = \mathbf{1} + k\bar{\beta})$): a) $\rho = -0.9$ b) $\rho = 0$.

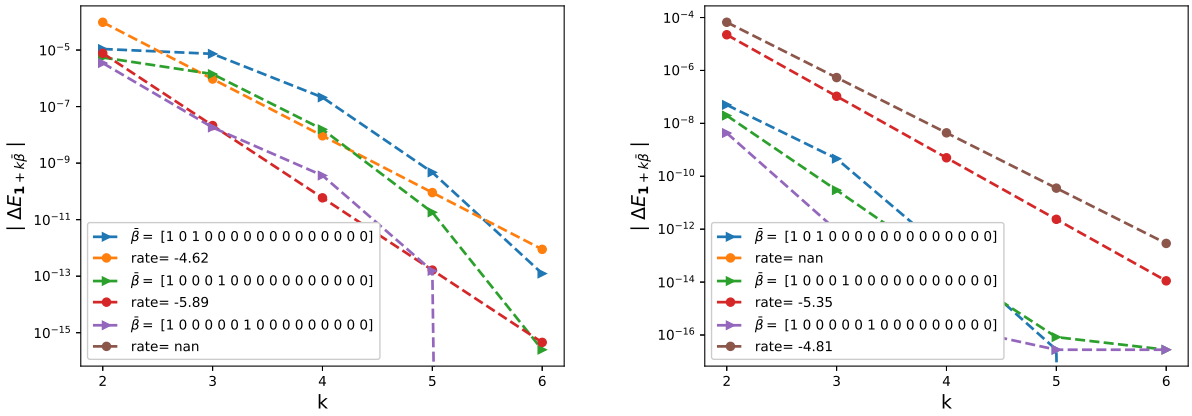

(a) (b)

Figure 44: The rate of convergence of mixed order differences $|\Delta E_\beta|$ $(\beta = \mathbf{1} + k\bar{\beta})$): a) $\rho = -0.9$ b) $\rho = 0$.

N=4, K=0.8

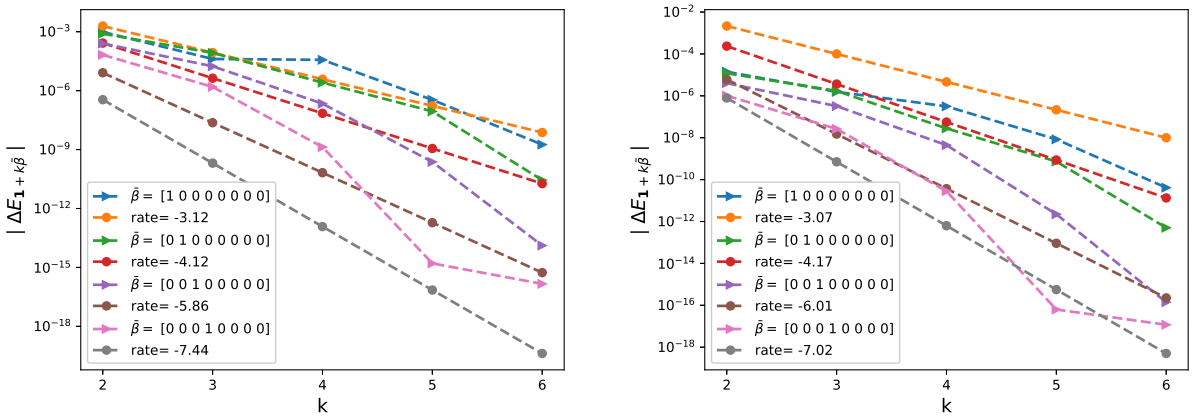

(a) (b)

Figure 45: The rate of convergence of first order differences $|\Delta E_\beta|$ ($\beta = \mathbf{1} + k\bar{\beta}$)): a) $\xi = 0.235^2$ b) $\xi = 10^{-5}$

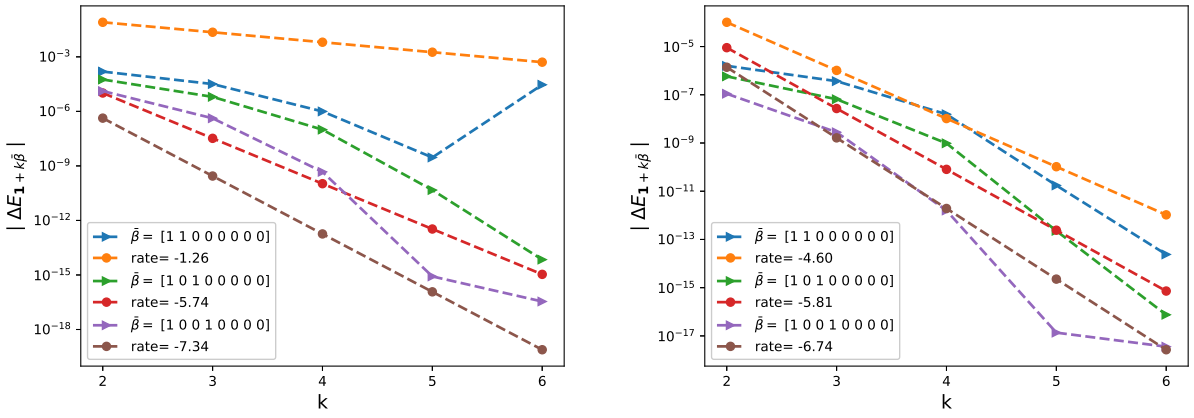

(a) (b)

Figure 46: The rate of convergence of mixed order differences $|\Delta E_\beta|$ ($\beta = \mathbf{1} + k\bar{\beta}$)): a) $\xi = 0.235^2$ b) $\xi = 10^{-5}$

N=8, K=0.8

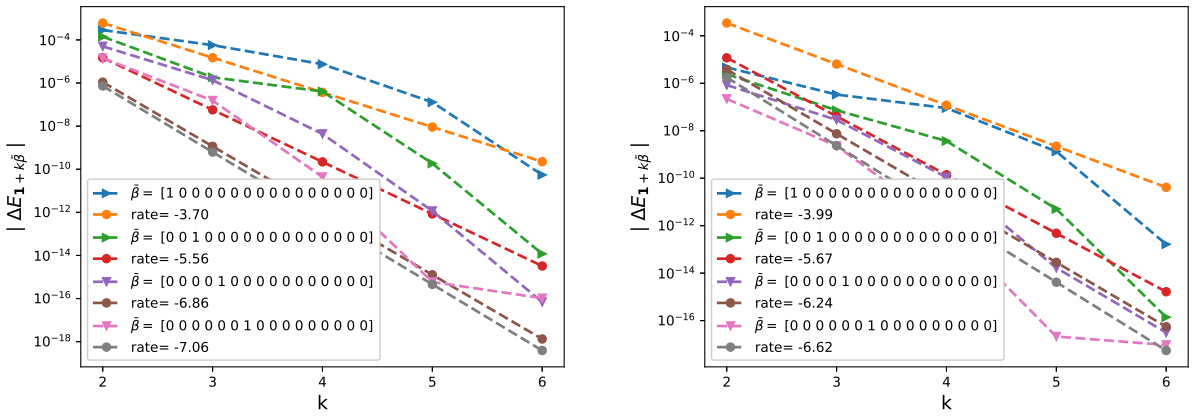

(a) (b)

Figure 47: The rate of convergence of first order differences $|\Delta E_\beta|$ $(\beta = \mathbf{1} + k\bar{\beta})$): a) $\xi = 0.235^2$ b) $\xi = 10^{-5}$

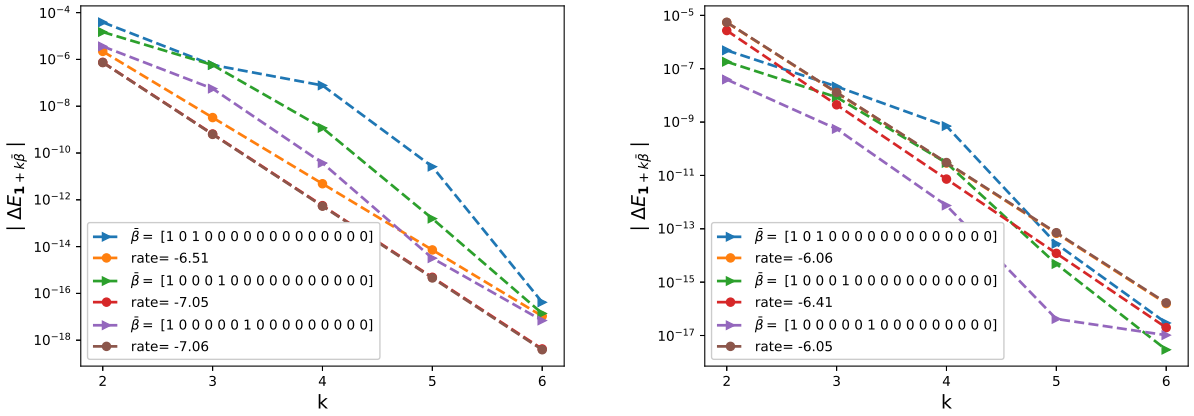

(a) (b)

Figure 48: The rate of convergence of mixed order differences $|\Delta E_\beta|$ $(\beta = \mathbf{1} + k\bar{\beta})$): a) $\xi = 0.235^2$ b) $\xi = 10^{-5}$

B.9 Investigating mixed differences wrt moneyness K

Case $H = 0.43$

$N = 8$

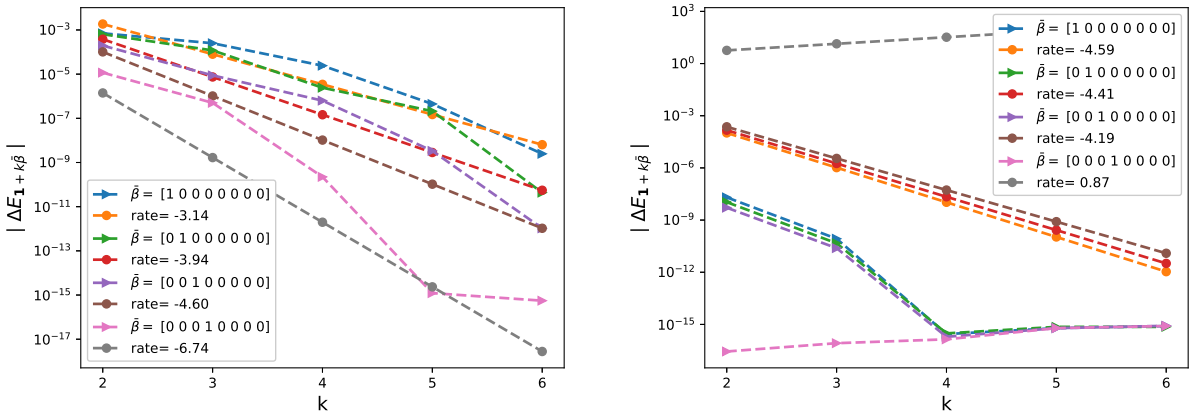

(a) (b)

Figure 49: The rate of convergence of first order differences $|\Delta E_\beta|$ ($\beta = \mathbf{1} + k\bar{\beta}$)): a) $\xi = 0.235^2$ b) $\xi = 10^{-5}$

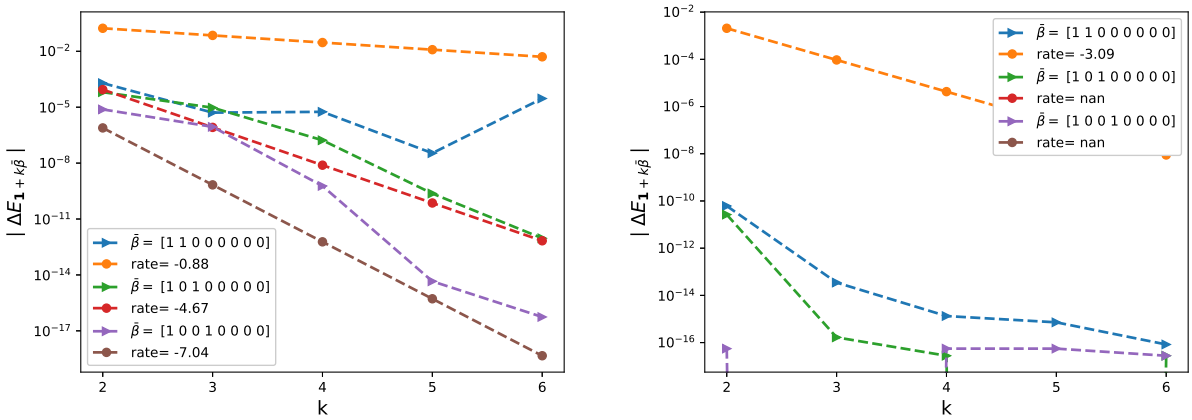

(a) (b)

Figure 50: The rate of convergence of mixed order differences $|\Delta E_\beta|$ ($\beta = \mathbf{1} + k\bar{\beta}$)): a) $\xi = 0.235^2$ b) $\xi = 10^{-5}$

$N = 16$

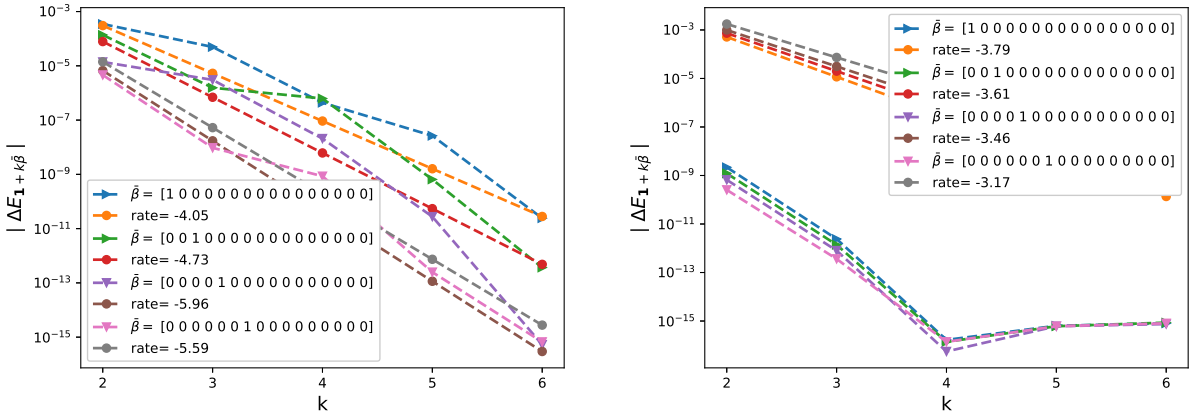

(a) (b)

Figure 51: The rate of convergence of first order differences $|\Delta E_\beta|$ $(\beta = \mathbf{1} + k\bar{\beta})$): a) $\xi = 0.235^2$ b) $\xi = 10^{-5}$

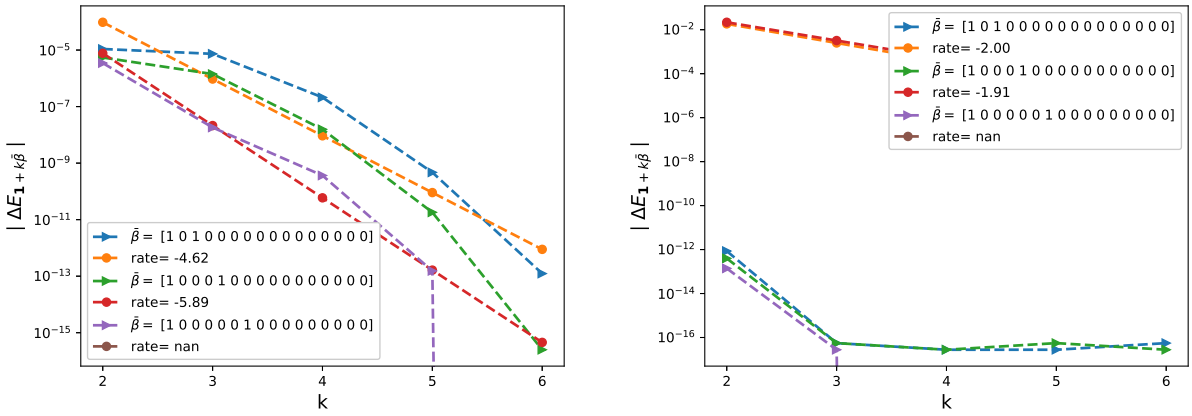

(a) (b)

Figure 52: The rate of convergence of mixed order differences $|\Delta E_\beta|$ $(\beta = \mathbf{1} + k\bar{\beta})$): a) $\xi = 0.235^2$ b) $\xi = 10^{-5}$

Case $H = 0.07$

$N = 8$

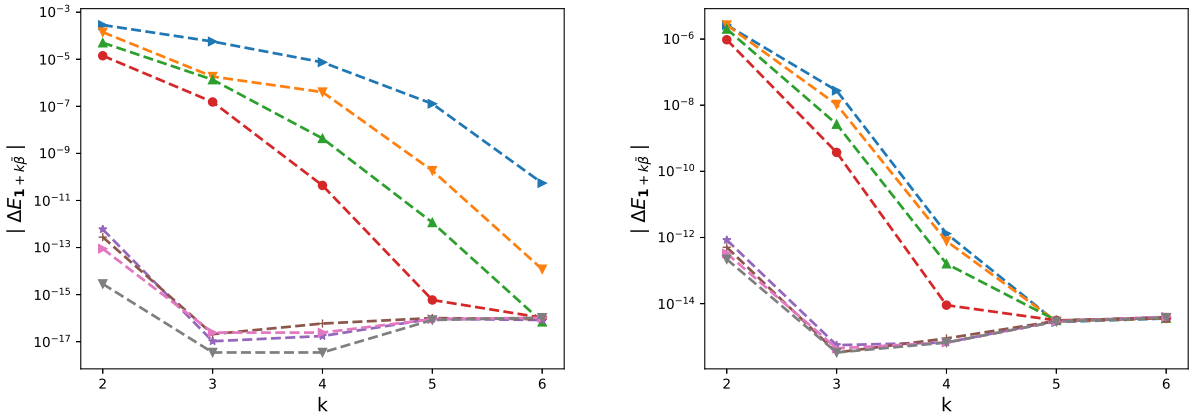

(a) (b)

Figure 53: The rate of convergence of first order differences $|\Delta E_\beta|$ ($\beta = \mathbf{1} + k\bar{\beta}$)): a) $K = 1$ b) $K = \exp(-4)$.

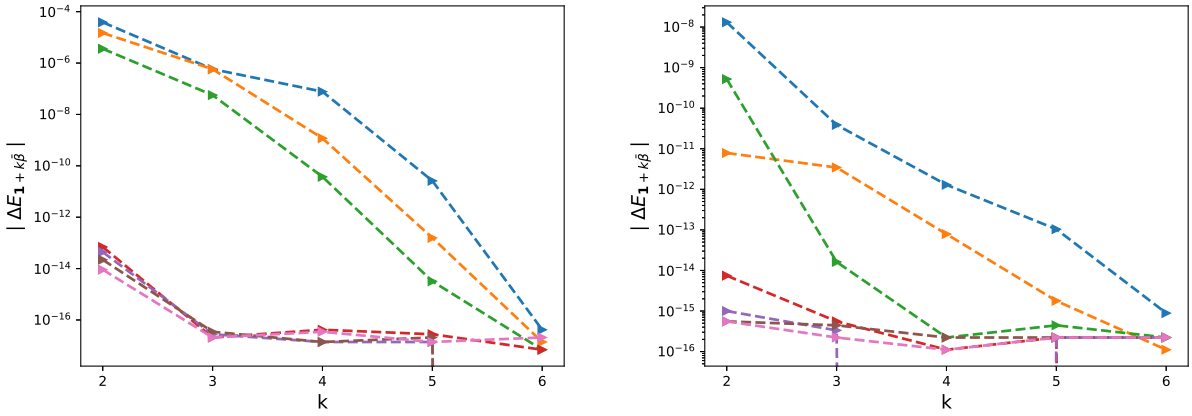

(a) (b)

Figure 54: The rate of convergence of second order differences $|\Delta E_\beta|$ ($\beta = \mathbf{1} + k\bar{\beta}$)): a) $K = 1$ b) $K = \exp(-4)$.

$N = 16$

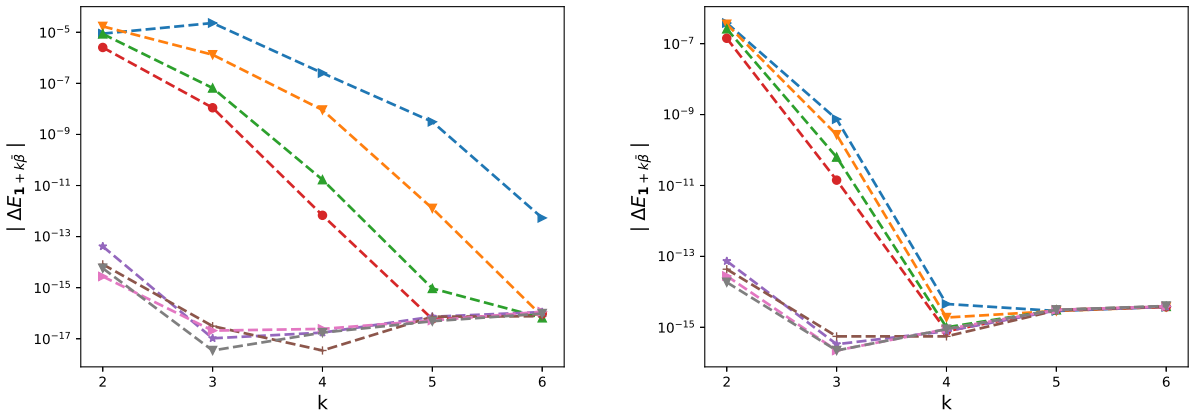

(a) (b)

Figure 55: The rate of convergence of first order differences $|\Delta E_\beta|$ ($\beta = \mathbf{1} + k\bar{\beta}$)): a) $K = 1$ b) $K = \exp(-4)$.

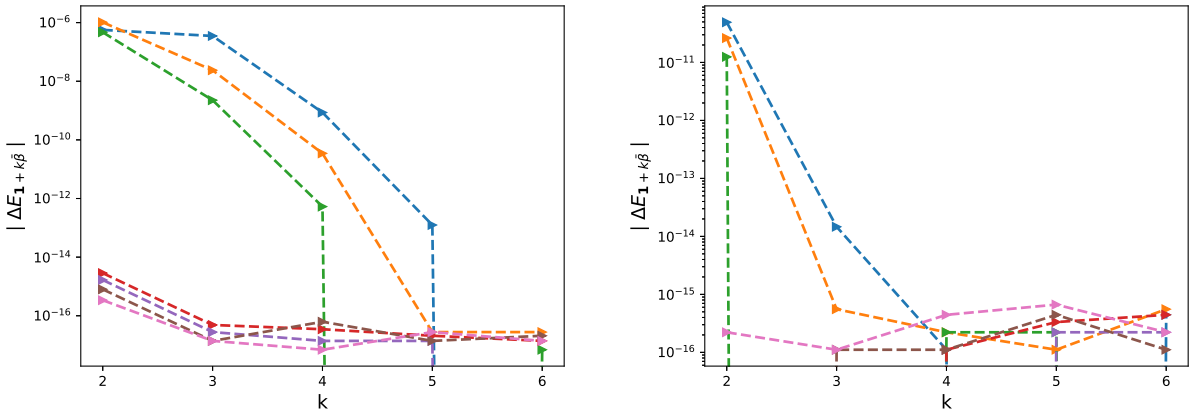

(a) (b)

Figure 56: The rate of convergence of second order differences $|\Delta E_\beta|$ ($\beta = \mathbf{1} + k\bar{\beta}$)): a) $K = 1$ b) $K = \exp(-4)$.

B.10 Convergence plots using MISC ($H = 0.43$)

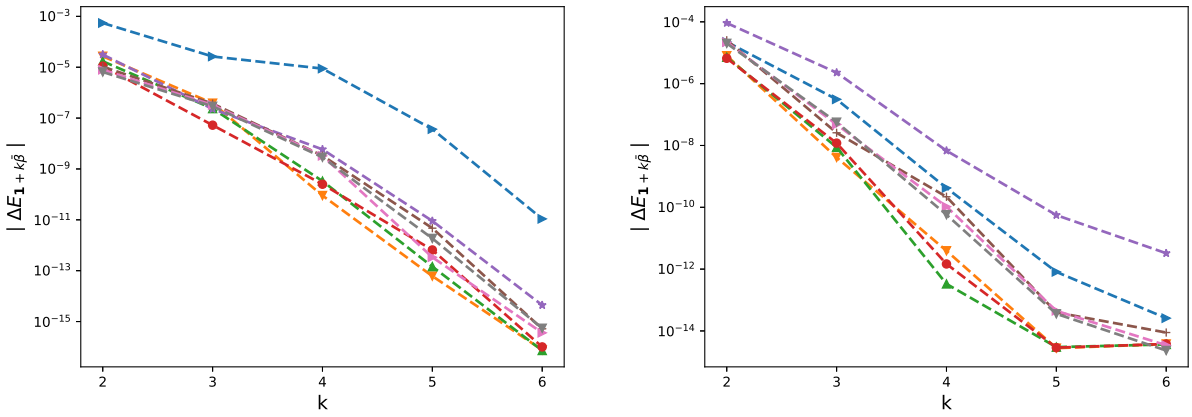

(a) (b)

Figure 57: The rate of convergence of first order differences $|\Delta E_\beta|$ ($\beta = \mathbf{1} + k\bar{\beta}$)): a) $K = 1$ b) $K = \exp(-4)$.

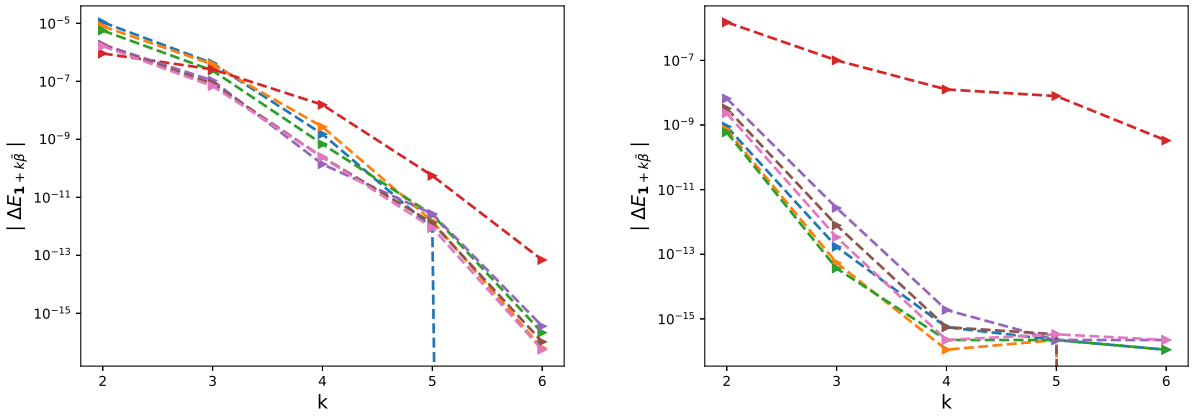

(a) (b)

Figure 58: The rate of convergence of second order differences $|\Delta E_\beta|$ ($\beta = \mathbf{1} + k\bar{\beta}$)): a) $K = 1$ b) $K = \exp(-4)$.

Case of 2 time steps, $K = e^{-4}$

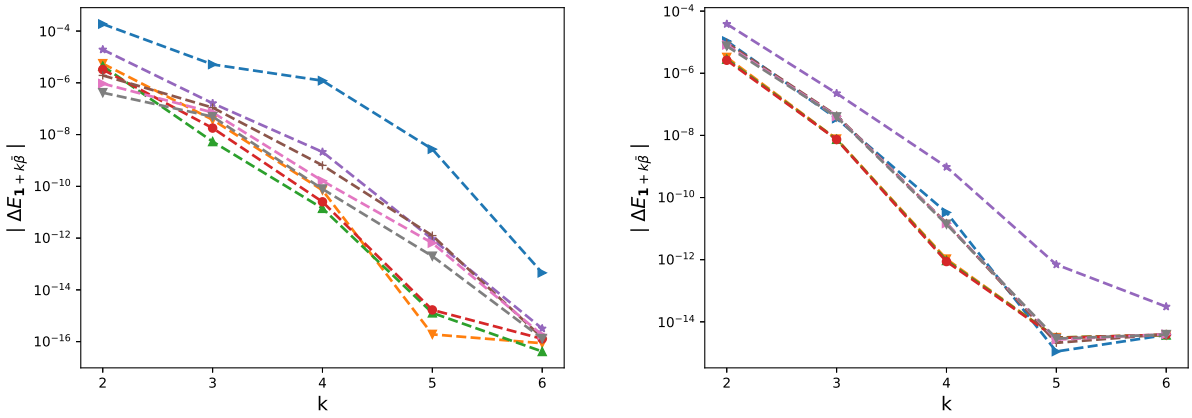

(a) (b)

Figure 59: The rate of convergence of first order differences $|\Delta E_\beta|$ ($\beta = \mathbf{1} + k\bar{\beta}$)): a) $K = 1$ b) $K = \exp(-4)$.

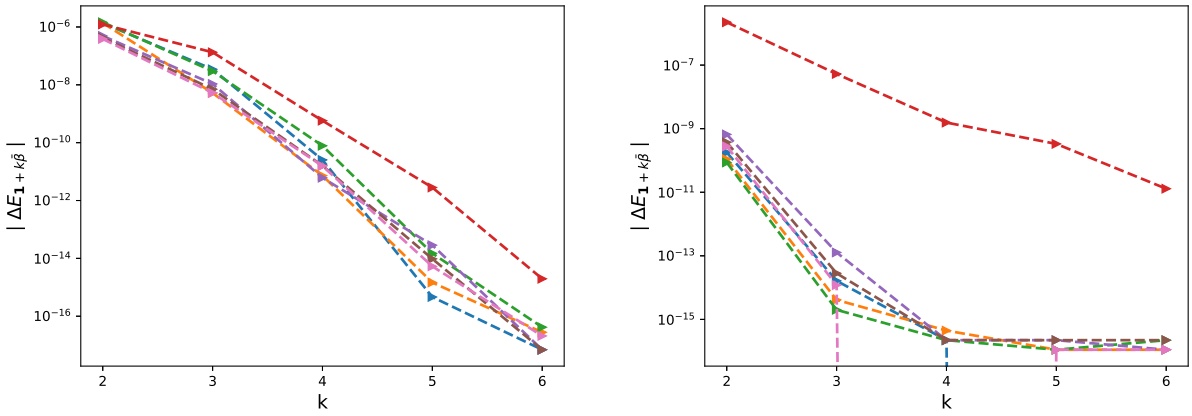

(a) (b)

Figure 60: The rate of convergence of second order differences $|\Delta E_\beta|$ ($\beta = \mathbf{1} + k\bar{\beta}$)): a) $K = 1$ b) $K = \exp(-4)$.

Case of 2 time steps, $K = 1.2$

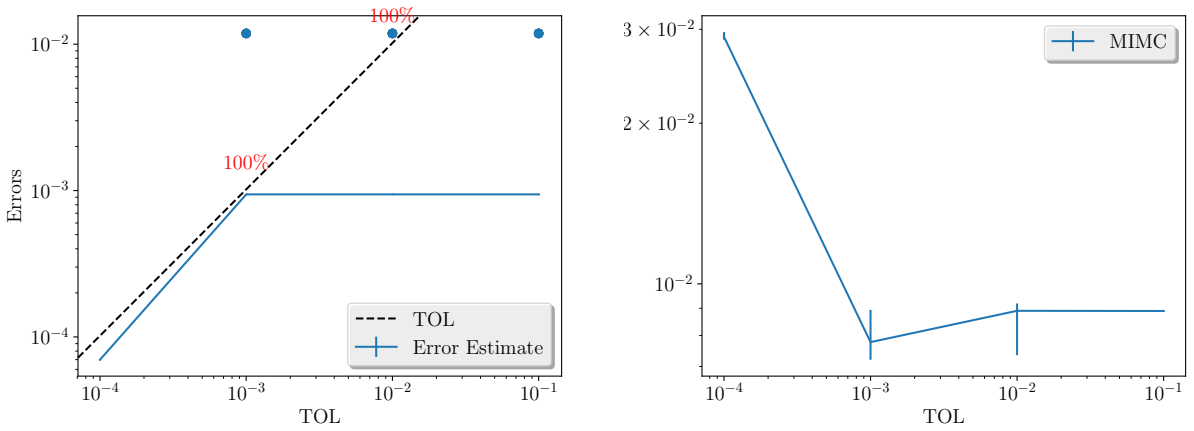

(a) Error estimate (b) Average running time as a function of TOL

Figure 61: Convergence and complexity results for the call payoff with rBergomi model.

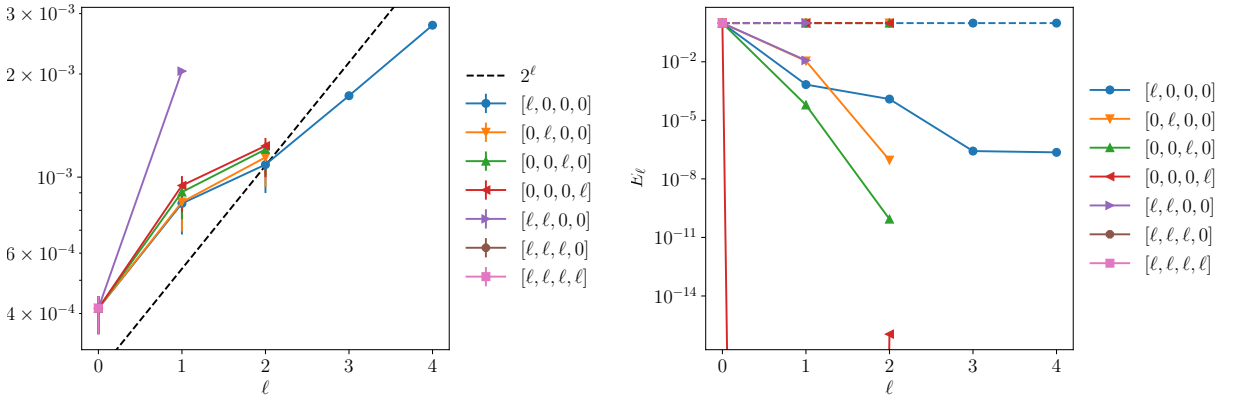

(a) Average Computational time per level (b) The convergence rate of mixed differences per level

Figure 62: Convergence and work rates for discretization levels the call payoff with rBergomi model.

Case of 4 time steps, $K = e^{-4}$

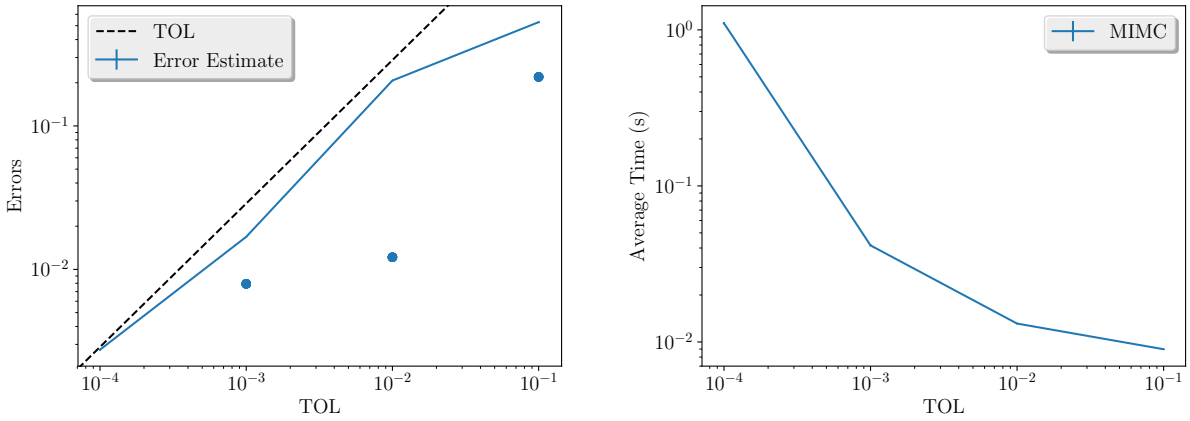

(a) Error estimate (b) Average running time as a function of TOL

Figure 63: Convergence and complexity results for the call payoff with rBergomi model.

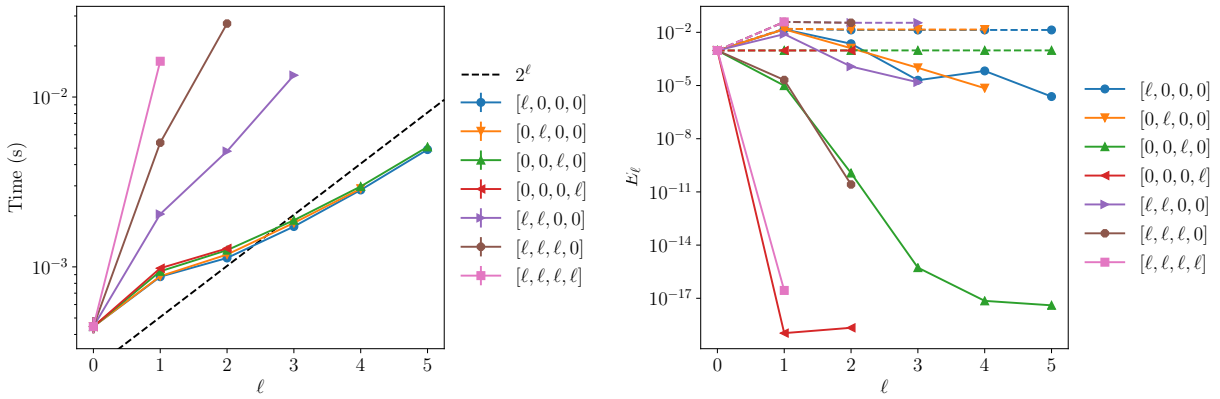

(a) Average Computational time per level (b) The convergence rate of mixed differences per level

Figure 64: Convergence and work rates for discretization levels the call payoff with rBergomi model.

Case of 4 time steps, $K = 1.2$

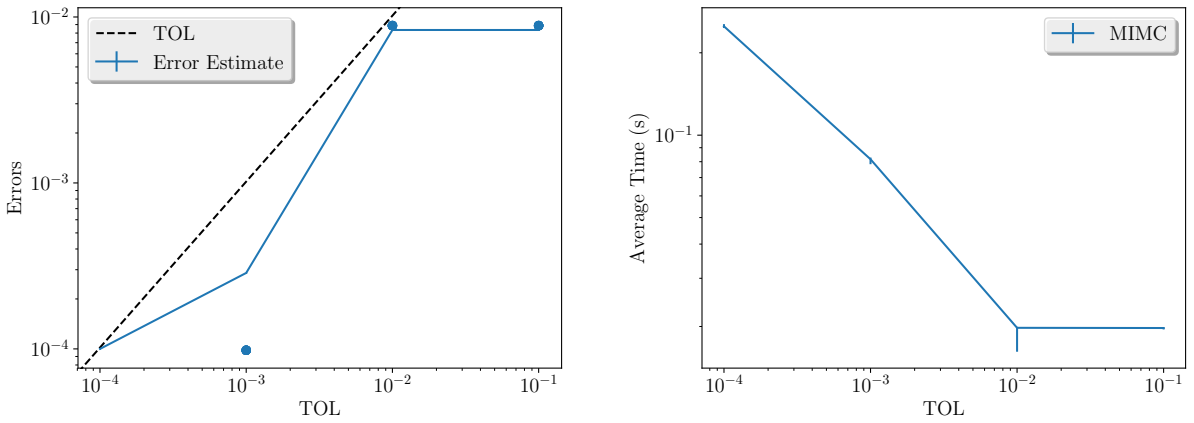

(a) Error estimate (b) Average running time as a function of TOL

Figure 65: Convergence and complexity results for the call payoff with rBergomi model.

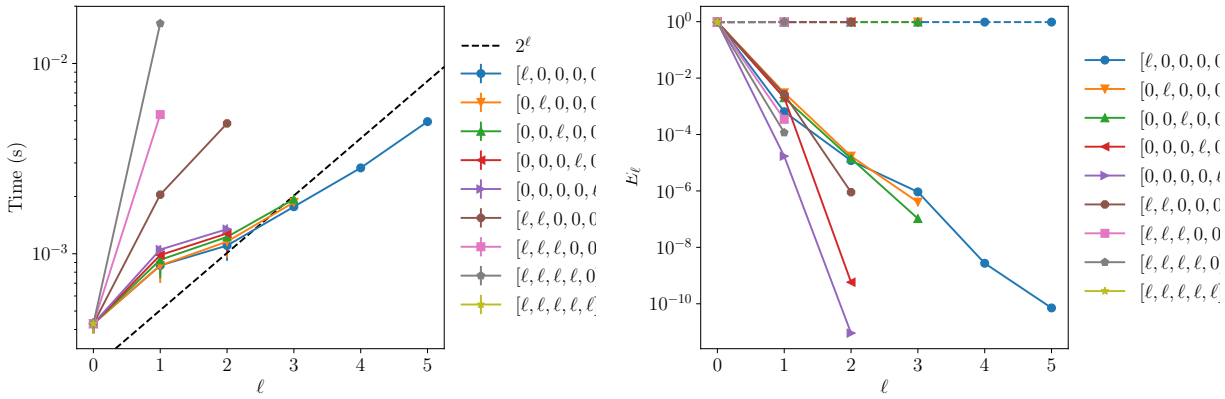

(a) Average Computational time per level (b) The convergence rate of mixed differences per level

Figure 66: Convergence and work rates for discretization levels the call payoff with rBergomi model.

Case of 8 time steps, $K = e^{-4}$

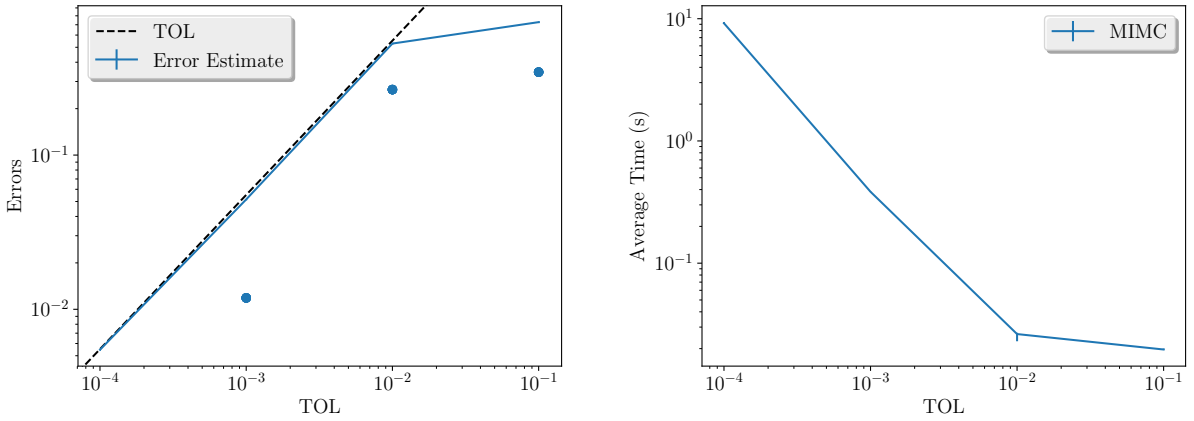

(a) Error estimate (b) Average running time as a function of TOL

Figure 67: Convergence and complexity results for the call payoff with rBergomi model.

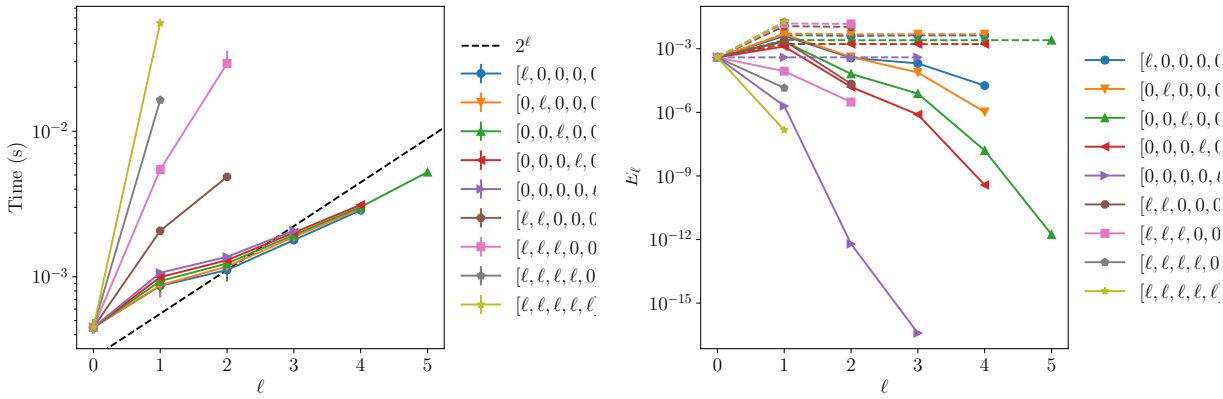

(a) Average Computational time per level (b) The convergence rate of mixed differences per level

Figure 68: Convergence and work rates for discretization levels the call payoff with rBergomi model.

Case of 8 time steps, $K = 1.2$

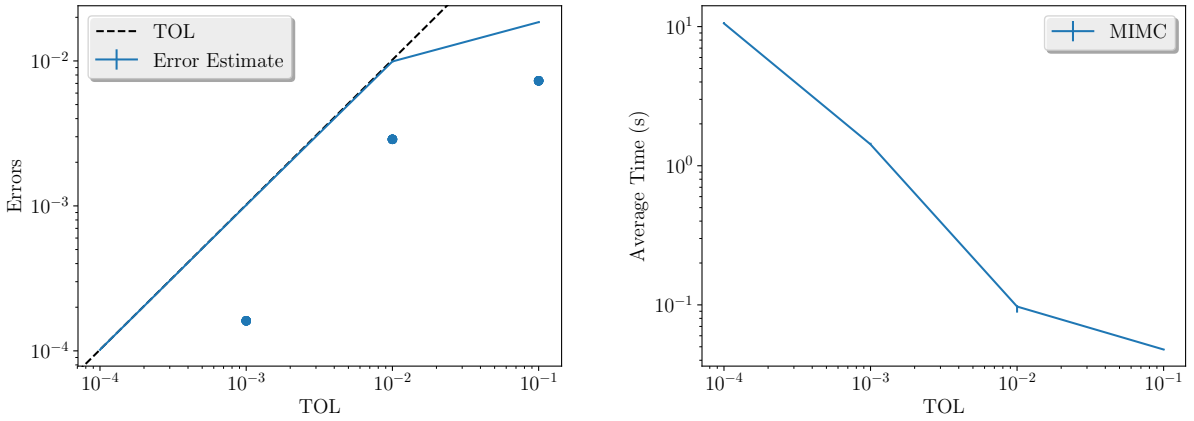

(a) Error estimate (b) Average running time as a function of TOL

Figure 69: Convergence and complexity results for the call payoff with rBergomi model.

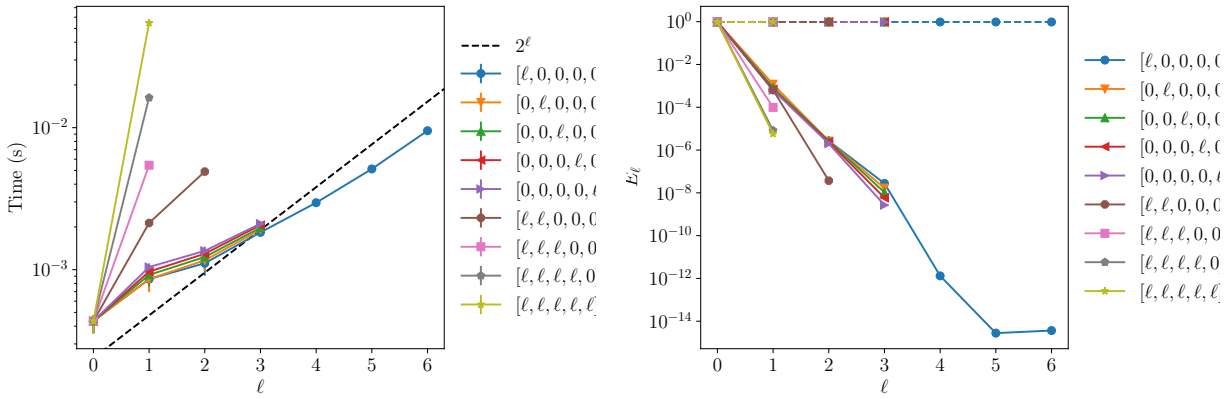

(a) Average Computational time per level (b) The convergence rate of mixed differences per level

Figure 70: Convergence and work rates for discretization levels the call payoff with rBergomi model.

Case of 16 **time steps,** $K = e^{-4}$

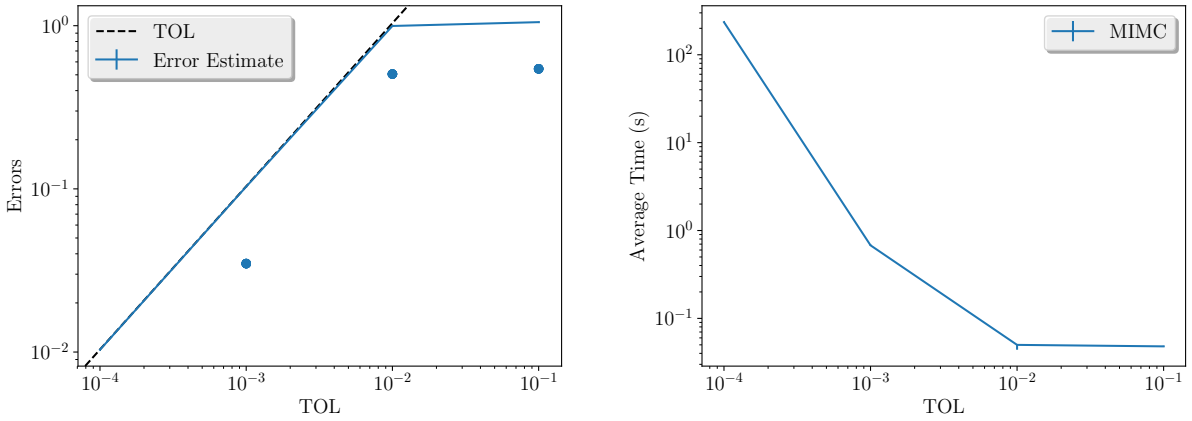

(a) Error estimate (b) Average running time as a function of TOL

Figure 71: Convergence and complexity results for the call payoff with rBergomi model.

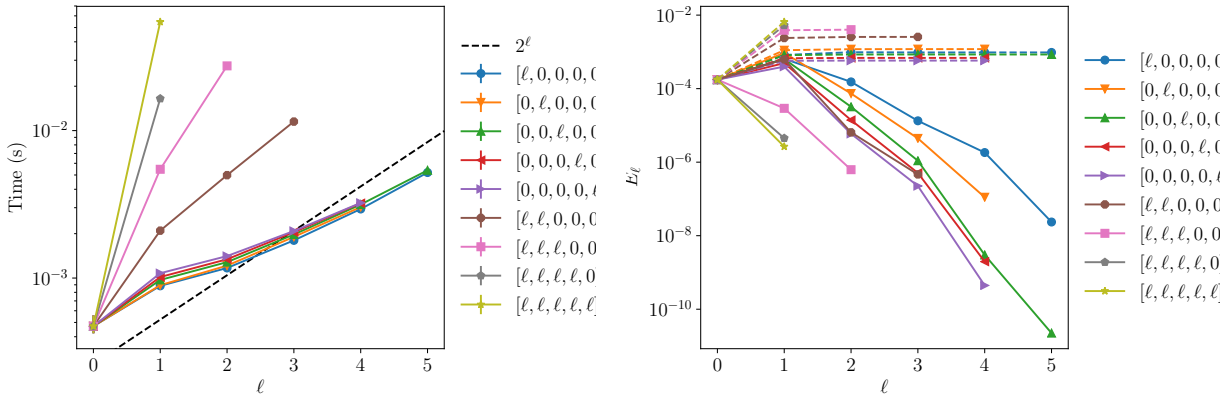

(a) Average Computational time per level (b) The convergence rate of mixed differences per level

Figure 72: Convergence and work rates for discretization levels the call payoff with rBergomi model.

Case of 16 **time steps,** $K = 1.2$

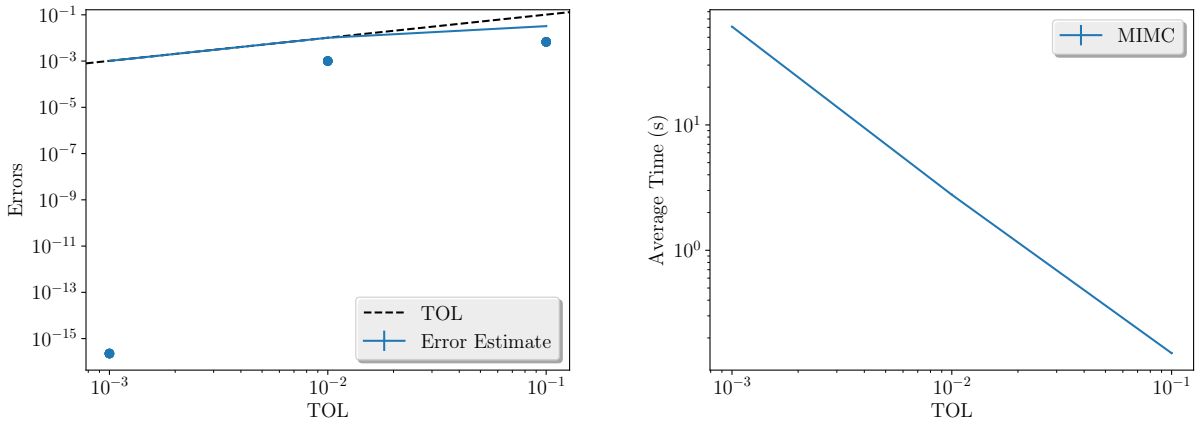

(a) Error estimate (b) Average running time as a function of TOL

Figure 73: Convergence and complexity results for the call payoff with rBergomi model.

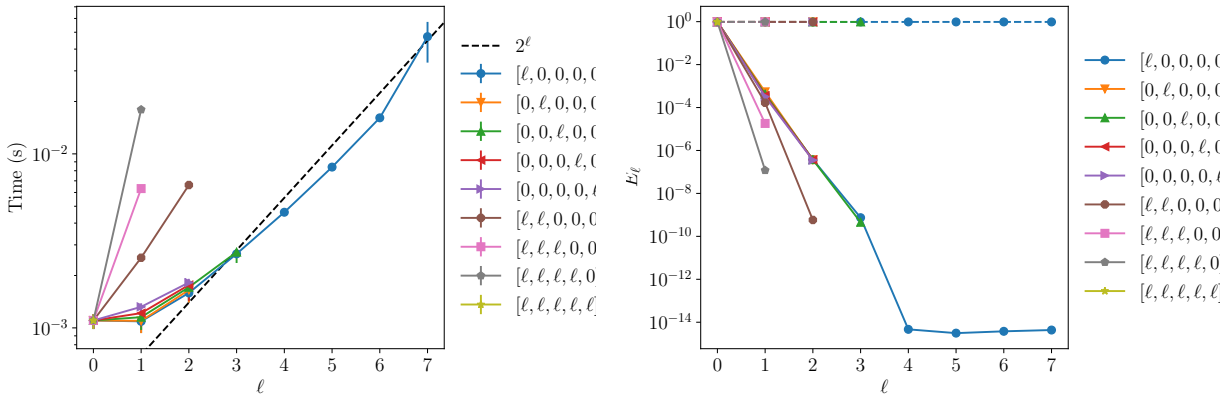

(a) Average Computational time per level (b) The convergence rate of mixed differences per level

Figure 74: Convergence and work rates for discretization levels the call payoff with rBergomi model.

B.11 MISC plots

B.12 Non Hierarchical

H=0.43

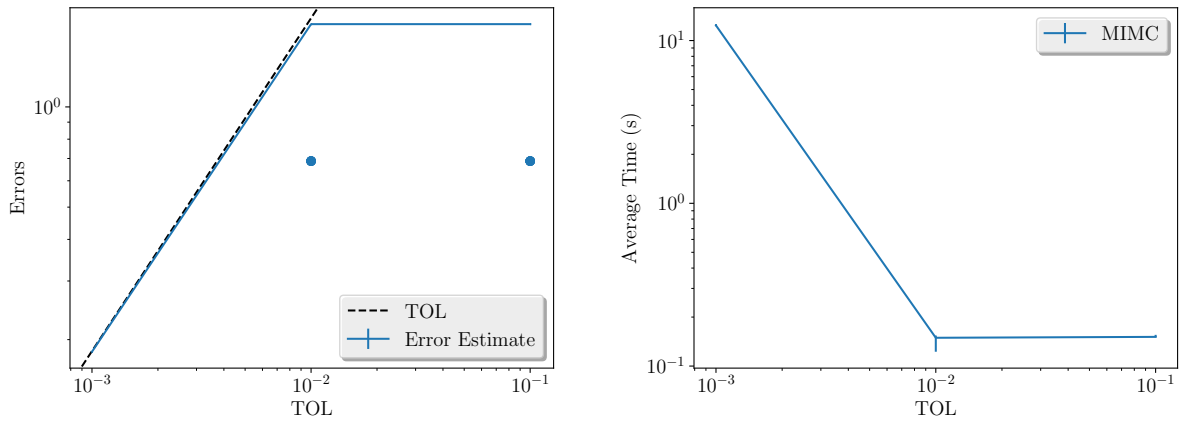

(a) Error estimate (b) Average running time as a function of TOL

Figure 75: Convergence and complexity results for the call payoff with rBergomi model.

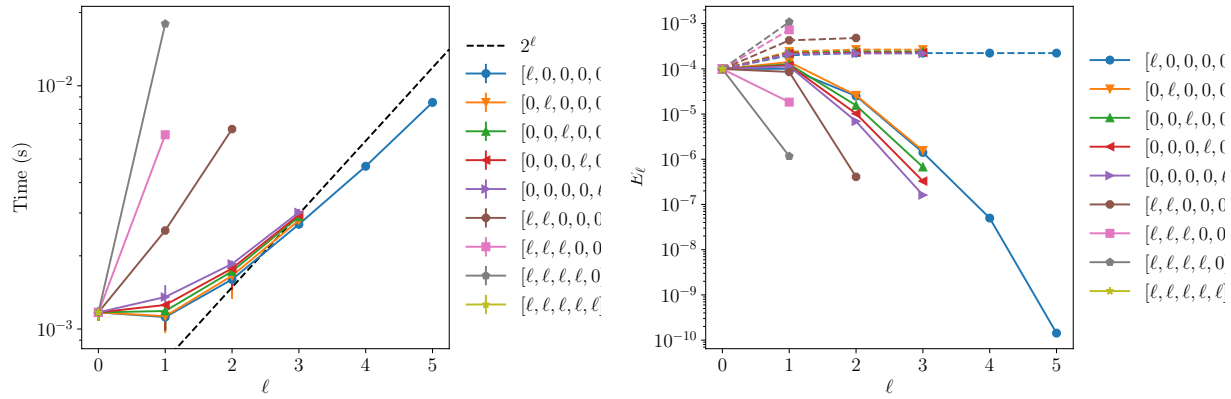

(a) Average Computational time per level (b) The convergence rate of mixed differences per level

Figure 76: Convergence and work rates for discretization levels the call payoff with rBergomi model.

Case of 8 time steps

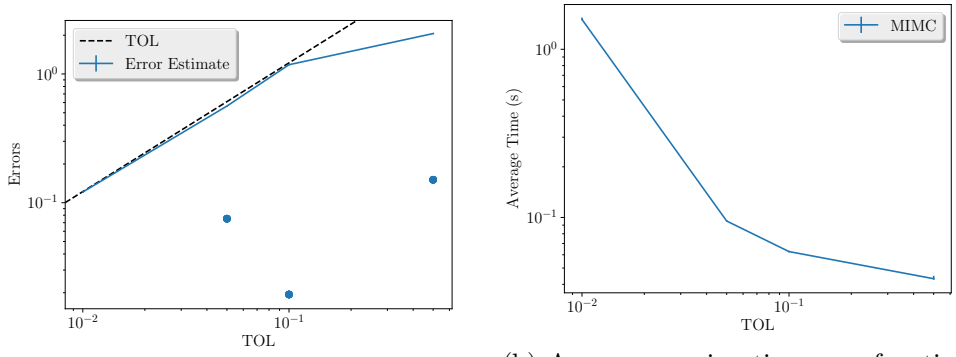

(a) Error estimate

(b) Average running time as a function of TOL

Figure 77: Convergence and complexity results for the call payoff with rBergomi model for $K = 1$, $H = 0.43$ and $N = 8$.

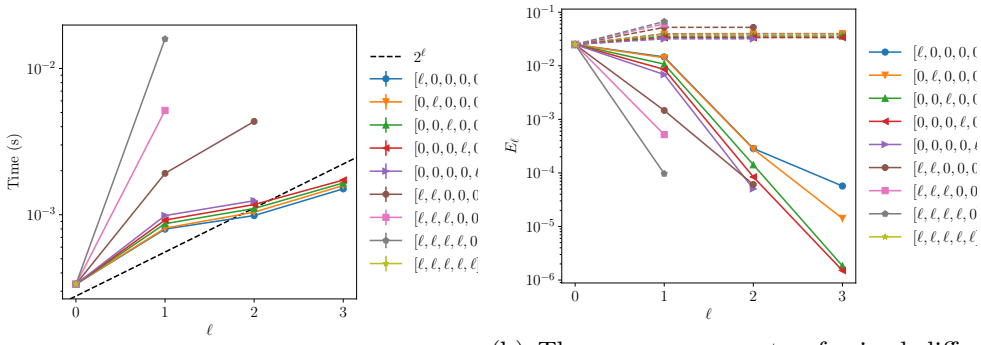

(a) Average Computational time per level

(b) The convergence rate of mixed differences per level

Figure 78: Convergence and work rates for discretization levels the call payoff with rBergomi model for $K = 1$, $H = 0.43$ and $N = 8$.

Case of 16 time steps

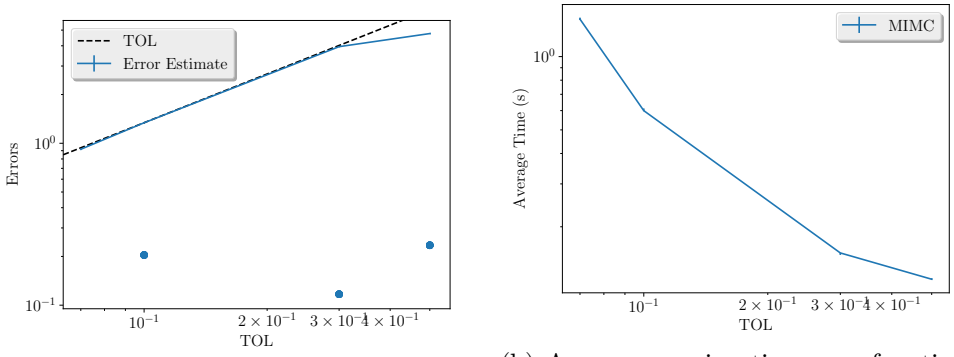

(a) Error estimate

(b) Average running time as a function of TOL

Figure 79: Convergence and complexity results for the call payoff with rBergomi model for $K = 1$, $H = 0.43$ and $N = 16$.

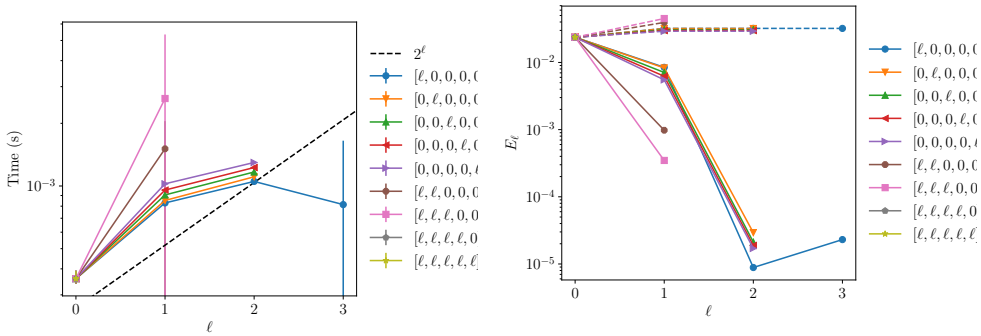

(a) Average Computational time per level

(b) The convergence rate of mixed differences per level

Figure 80: Convergence and work rates for discretization levels the call payoff with rBergomi model for $K = 1$, $H = 0.43$ and $N = 16$.

H=0.07

Case of 8 time steps

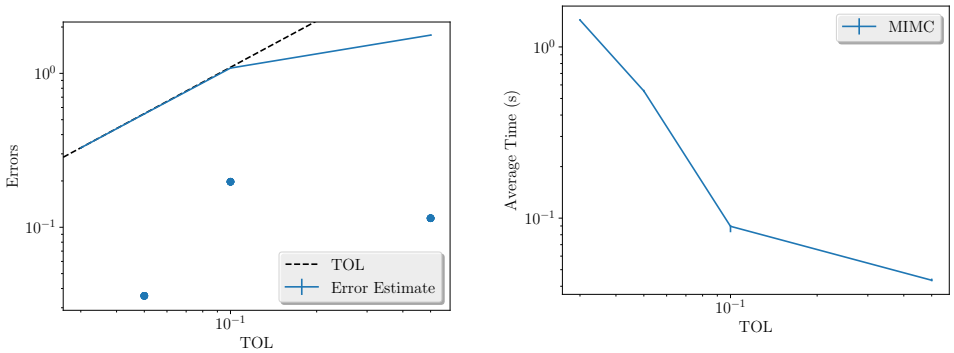

(a) Error estimate

(b) Average running time as a function of TOL

Figure 81: Convergence and complexity results for the call payoff with rBergomi model for $K = 1$, $H = 0.07$ and $N = 8$.

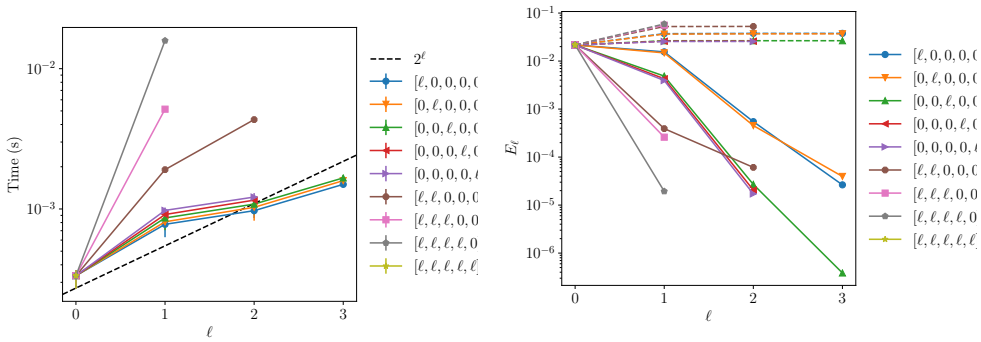

(a) Average Computational time per level

(b) The convergence rate of mixed differences per level

Figure 82: Convergence and work rates for discretization levels the call payoff with rBergomi model for $K = 1$, $H = 0.07$ and $N = 8$.

Case of 16 time steps

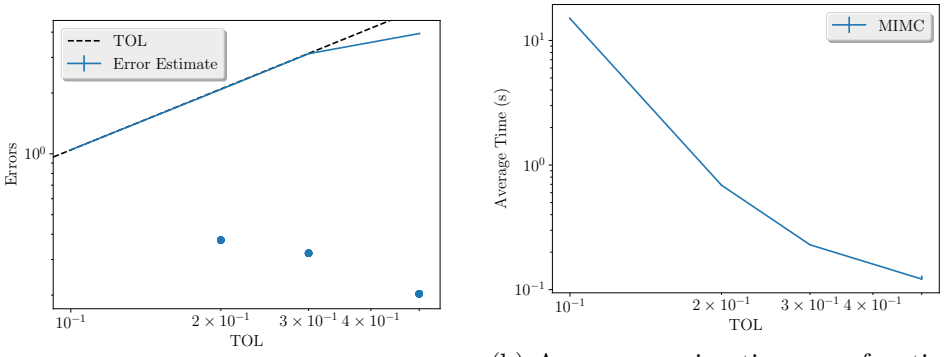

(a) Error estimate

(b) Average running time as a function of TOL

Figure 83: Convergence and complexity results for the call payoff with rBergomi model for $K = 1$, $H = 0.07$ and $N = 16$.

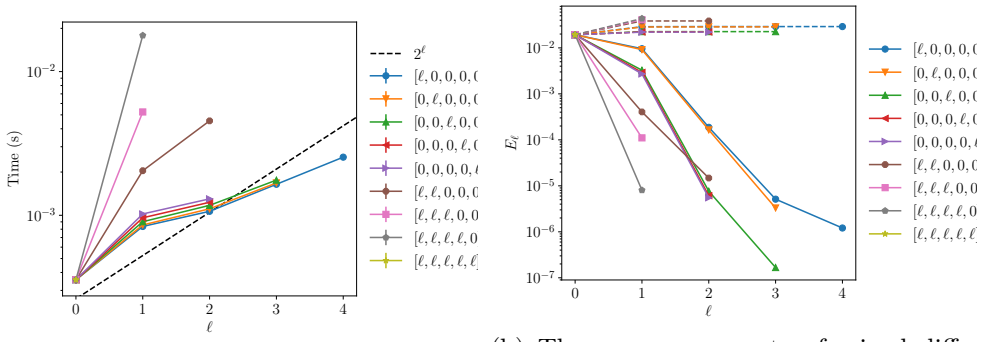

(a) Average Computational time per level

(b) The convergence rate of mixed differences per level

Figure 84: Convergence and work rates for discretization levels the call payoff with rBergomi model for $K = 1$, $H = 0.07$ and $N = 16$.

B.13 Hierarchical

H=0.43

Case of 8 time steps

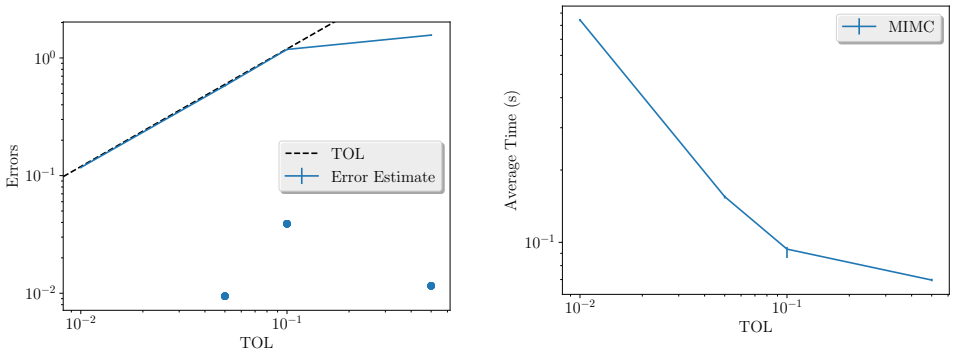

(a) Error estimate

(b) Average running time as a function of TOL

Figure 85: Convergence and complexity results for the call payoff with rBergomi model for $K = 1$, $H = 0.43$ and $N = 8$.

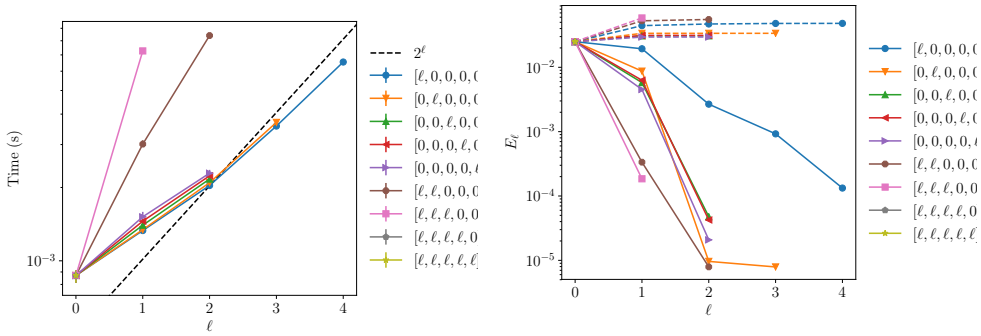

(a) Average Computational time per level

(b) The convergence rate of mixed differences per level

Figure 86: Convergence and work rates for discretization levels the call payoff with rBergomi model for $K = 1$, $H = 0.43$ and $N = 8$.

Case of 16 time steps

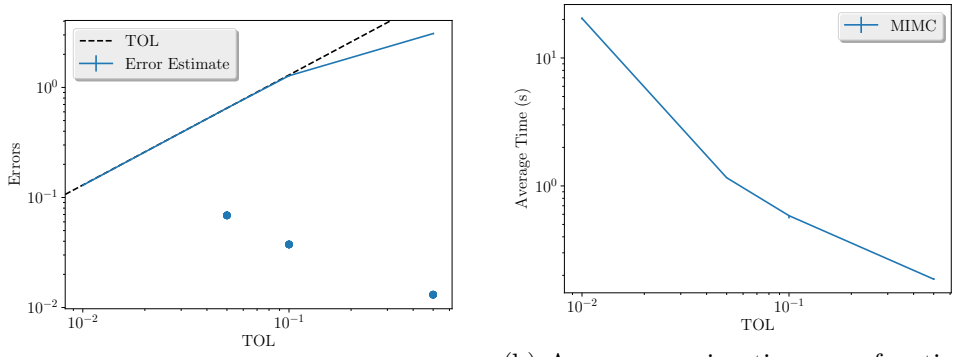

(a) Error estimate

(b) Average running time as a function of TOL

Figure 87: Convergence and complexity results for the call payoff with rBergomi model for $K = 1$, $H = 0.43$ and $N = 16$.

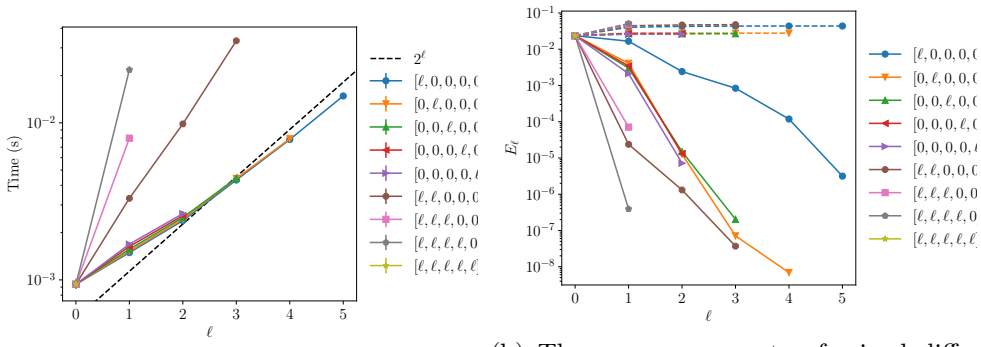

(a) Average Computational time per level

(b) The convergence rate of mixed differences per level

Figure 88: Convergence and work rates for discretization levels the call payoff with rBergomi model for $K = 1$, $H = 0.43$ and $N = 16$.

H=0.07

Case of 8 time steps

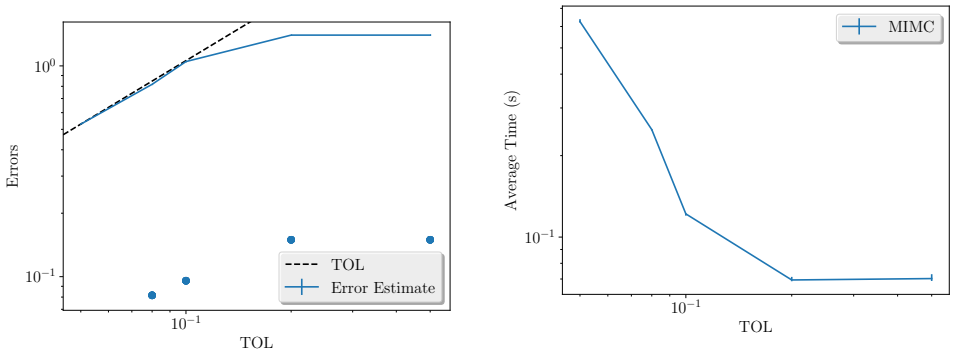

(a) Error estimate

(b) Average running time as a function of TOL

Figure 89: Convergence and complexity results for the call payoff with rBergomi model for $K = 1$, $H = 0.07$ and $N = 8$.

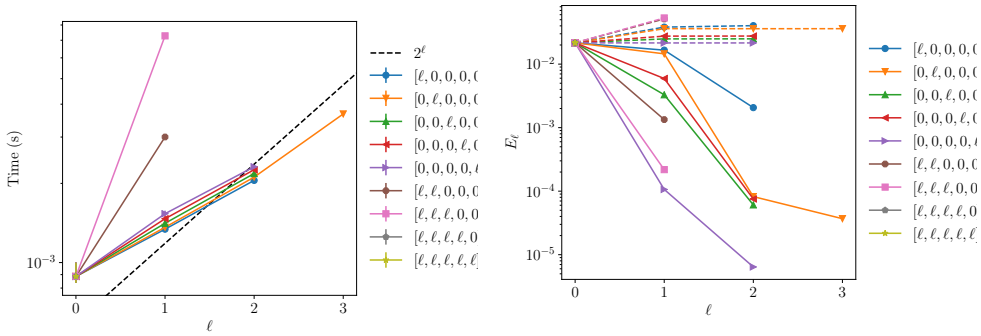

(a) Average Computational time per level

(b) The convergence rate of mixed differences per level

Figure 90: Convergence and work rates for discretization levels the call payoff with rBergomi model for $K = 1$, $H = 0.07$ and $N = 8$.

Case of 16 time steps

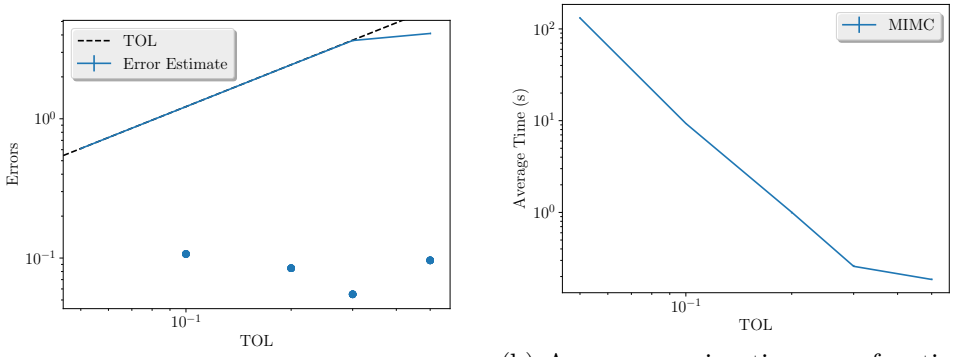

(a) Error estimate

(b) Average running time as a function of TOL

Figure 91: Convergence and complexity results for the call payoff with rBergomi model for $K = 1$, $H = 0.07$ and $N = 16$.

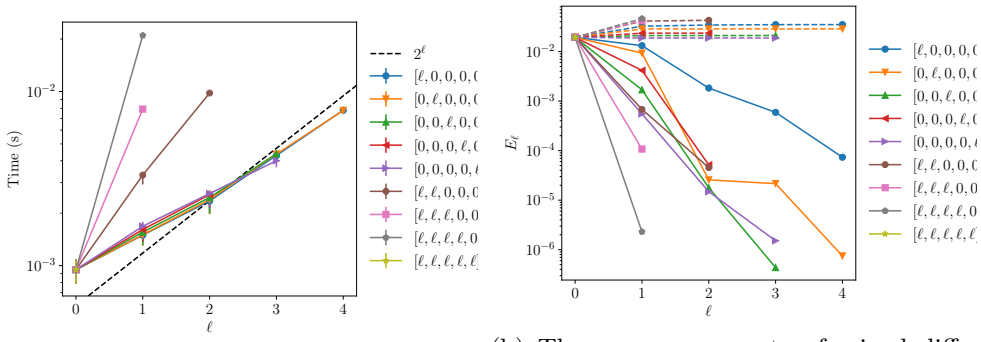

(a) Average Computational time per level

(b) The convergence rate of mixed differences per level

Figure 92: Convergence and work rates for discretization levels the call payoff with rBergomi model for $K = 1$, $H = 0.07$ and $N = 16$.